Am J Transl Res 2024;16(9):4355-4378
www.ajtr.org /ISSN:1943-8141/AJTR0156374

Original Article

Construction and validation of immune-associated lncRNA model for predicting immune status and therapeutic reactions of triple-negative breast cancer

Yaqian Liu[1*], Ming Zhang[2*], Jie Sun[1*], Jinyuan Zhang[1], Boshi Gu[1], Jun Li[1], Bo Pan[1], Haidong Zhao[1]

[1]Department of Breast Surgery, The Second Affiliated Hospital of Dalian Medical University, Dalian, Liaoning, China; [2]Department of Pharmacy, The Second Affiliated Hospital of Dalian Medical University, Dalian, Liaoning, China. [*]Equal contributors.

Received March 5, 2024; Accepted July 17, 2024; Epub September 15, 2024; Published September 30, 2024

Abstract: Objective: The immune status of the tumor microenvironment significantly impacts the clinical prognosis of triple-negative breast cancer (TNBC). The involvement of long noncoding RNAs (lncRNAs) in tumor immune infiltration is widely acknowledged. Therefore, it is crucial to explore the role of significant immune-related lncRNAs in TNBC. Methods: We acquired RNA, single-cell sequencing, and clinical information on TNBC from The Cancer Genome Atlas (TCGA) and the Gene Expression Omnibus (GEO) databases. To identify immune-related lncRNAs, immune infiltration subgroups were determined and verified using single-sample gene-set enrichment analysis, non-negative matrix factorization, and weighted gene co-expression network analysis. CIBERSORTx, deconvolution, drug sensitivity, and Scissor analyses revealed that differences in cell type and drug efficacy were associated with immune grouping. Results: TNBC samples were classified into immune-desert (cold) and immune-inflamed (hot) subgroups based on a lncRNA model (including LINC01550, LY86-AS1, LINC00494, LINC00877, CHRM3-AS2, HCP5, MIR155HG, and PIK3CD-AS1). Furthermore, using in vitro experiments, we found that LINC01550 promoted malignant phenotypes, including proliferation, survival, and migration of TNBC. The immune-inflamed subgroup exhibited significantly lower half-maximal inhibitory concentration values for common anti-tumor drugs, including palbociclib, ribociclib, mitoxantrone, and sorafenib (T-test, $P < 0.001$). This may be related to the fact that the immune-inflamed subgroup has more plasmacytoid dendritic cells (pDCs) and B cells than those in immune-desert subgroups ($P < 0.001$). Conclusions: Differences in specific cell infiltration can lead to increased sensitivity of the immune-inflamed subgroup to anti-tumor drugs. The proposed lncRNA model holds great promise to assess the immune landscapes and therapeutic reactions of TNBC patients.

Keywords: LncRNA, triple negative breast cancer, immune model, immune infiltration, drug sensitivity

Introduction

Triple-negative breast cancer (TNBC) comprises approximately 20% of all breast cancer subtypes, as it lacks targeted therapies it exhibits heightened aggressiveness and an unfavorable prognosis compared with non-TNBC [1]. Although individuals with early-stage TNBC typically exhibit favorable responses to chemotherapy, the lack of effective treatment targets and regimens results in suboptimal median overall survival of patients with metastatic tumors of less than 1 year [2]. Compared with other subtypes of breast cancer, TNBC is characterized by lack of overexpression of estrogen and progesterone receptors (ER/PR) and human epidermal growth factor receptor 2 (HER2) biomarkers. This absence leads to poorer outcomes and inapplicability of targeted therapies. Therefore, traditional chemotherapy and radiotherapy are still the main treatment options for TNBC. Given the need for more effective targeted therapeutic options for this refractory disease, scientists are committed to characterizing the oncological molecular signatures of TNBC. Recent literature has shown that TNBC exhibits strong individual heterogeneity in the clinical, histopathological, molecular and tumor microenvironment. It can be divided into smaller categories, including basal-like

https://doi.org/10.62347/VIXN9362

(BL), mesenchymal stem cell-like (MSL), mesenchymal-like (M) and luminal androgen receptor type (LAR) [2]. However, while these specific biomarkers reflect the biological heterogeneity of TNBC, they still lack effective guidance for clinical strategies. Consequently, there is an urgent need to establish novel predictive biomarkers for TNBC patients and to explore more accurate diagnostic and therapeutic strategies in clinical practice.

The clinical outcomes of cancer patients have been extensively demonstrated to be significantly influenced by the tumor microenvironment phenotype in multiple research studies. The tumor immune microenvironment can be classified into two main categories: immune-desert (cold) and immune-inflamed (hot). The "cold" tumor phenotype is associated with immune failure, characterized by T-cell dysfunction and limited effectiveness of immunotherapeutic interventions [3, 4]. Therefore, identification of "hot" tumors and the conversion of "cold" tumors into the "hot" phenotype are crucial to enhance the efficacy of clinical interventions [5]. Consequently, development of novel biomarkers to characterize tumor immune status, as well as the establishment of immune risk models for patients with TNBC, are essential for prognostication and treatment optimization.

The involvement of long noncoding RNAs (lncRNAs) in diverse biological processes (including transcriptional, post-transcriptional, and epigenetic mechanisms) associated with tumor development has been well established. Recent studies have shown that lncRNAs are intricately involved in cancer immune regulation, influencing antigen release and presentation, immune cell infiltration, and immune activation and escape [6, 7]. Numerous prior studies have demonstrated the heightened capacity of lncRNAs to serve as immune microenvironment and prognostic biomarkers compared with that of protein-coding genes. This finding is primarily interrelated with the observation that immune-related lncRNAs exhibit specific expression modes within immune cells [8, 9]. In the tumor microenvironment, lncRNAs directly or indirectly regulate the expression levels of specific downstream genes through a variety of mechanisms, and play irreplaceable roles in the tumor immune process, including anti-inflammatory/pro-inflammatory directional polarization of macrophages, activation and depletion of CD8+ T lymphocytes, differentiation, development, and apoptosis of helper T lymphocytes [10-12]. LncRNAs often affect tumor immune surveillance, the immune response and other processes by regulating regulatory T cells and cytotoxic T lymphocytes, contributing to the formation of the immunosuppressive tumor microenvironment and promoting the malignant phenotype of tumor cells. These crucial lncRNAs participate in multiple signaling pathways of the tumor microenvironment and promote the proliferation and differentiation of regulatory T cells, so they may serve as potential therapeutic targets in clinical settings [13, 14]. Some lncRNAs have been found to be involved in the upregulation of CD8+ T lymphocytes and CD4+ Th1 cells, while inducing the downregulation of regulatory cells [15, 16]. Studies have found that lncRNAs can also regulate the differentiation of Treg cells by competitively binding microRNAs [15, 16]. For example, the expression of lncRNA SNHG1 in CD4+ T lymphocyte infiltrating tumors is significantly higher than that in peripheral blood CD4+ T lymphocytes, and it promotes IDO expression by competitively binding to miR-448, inducing more regulatory T cells to differentiate and mature, facilitating immune escape of breast cancer [16]. However, the precise roles of immune-specific lncRNAs in governing the dynamic interplay among cells within the tumor immune microenvironment, as well as their potential for predicting the therapeutic response of TNBC, remain largely unexplored.

In this study, we successfully established a lncRNA model containing eight molecules that could effectively indicate the immune status of TNBC. Then, we investigated the characteristics of the immune microenvironment, cell infiltration states, and disparities in drug sensitivity in the "hot" and "cold" subgroups based on the crucial lncRNA signature. Additionally, we found that LINC01550, as a differentially expressed lncRNA in TNBC, could mediate the proliferation and migration characteristics of tumors. Our results demonstrated that new potential immune-related lncRNA biomarkers might provide a reliable tool to guide clinical management of patients with TNBC.

Materials and methods

Acquisition and analysis of public bioinformatic data

TNBC transcriptomic data, which had been normalized using a $\log_2$(count+1) transformation, were obtained from the TCGA database, and the relevant clinical data were obtained through the UCSC Xena Browser. Additionally, the GSE58812 microarray matrices and their relevant clinical data were derived from the GEO database. LncRNA and mRNA expression were re-annotated using the biomaRt package of R (version 2.54.0) [17]. Information pertaining to immune-associated lncRNAs and pathways was acquired from the ImmLnc database and processed using the ImmuLncRNA (version 0.1.0) R package [18].

Tumor immune-infiltrating analysis

We used the R language ConsensusClusterPlus package (version 1.62.0) [19] for consistency clustering. Principal component analysis and the NbClust package (version 3.0.1) were used to calculate the optimal cluster number [20]. The tumor subgroups, classified as "cold" or "hot" based on the optimal cluster number, were subjected to clustering using t-distributed stochastic neighbor embedding (tSNE) dimensionality reduction. The single-sample gene-set enrichment analysis (ssGSEA) was employed to assess the collaborative changes of genes within specific gene sets in individual samples. Using the Tumor-immune System Interactions and Drug Bank database [21], we acquired the gene signatures of 28 tumor-infiltrating lymphocytes (TILs) (Table S1). The GSVA package of R (version 1.46.0) was utilized to conduct ssGSEA analysis [22], resulting in the calculation of enrichment scores for each sample, representing the abundance of the 28 distinct types of TILs. To ensure the dependability and coherence of the ssGSEA outcomes, six additional algorithms (quanTIseq, xCell, TIMER, ESTIMATE, MCP-counter, and EPIC) were employed for validation purposes [23-25].

Differential gene enrichment analysis

The limma package of R (version 3.54.1) was employed to filter the differentially expressed genes (DEGs) [26] based on the criterion of $|\log_2 FC| > 1.5$, with an additional requirement of an adjusted p-value < 0.05. Gene Ontology (GO) analysis, Kyoto Encyclopedia of Genes and Genomes (KEGG) enrichment analysis, and gene-set enrichment analysis (GSEA) of gene function and pathways were performed using the clusterProfiler package of R (version 4.6.0) [27]. Significant GSEA enrichment results were visualized using the GseaVis package (version 0.0.5) [28]. Other detailed results are listed in Table S1.

Construction of co-expression lncRNA networks

The weighted gene co-expression network analysis (WGCNA) algorithm (version 1.7) of R systematically integrates coordinated gene populations into gene modules and investigates their association with dominant phenotypes [29, 30]. The soft threshold β was set to 6. The topological overlap matrix (TOM) and corresponding dissimilarity (1-TOM) were generated using WGCNA. The lncRNA module identified that a dynamic tree-cutting approach exhibited the highest correlation with the immune phenotype, which was chosen for further investigation. The immune-related lncRNAs were identified as those exhibiting high gene significance and module membership. The Survminer package (version 0.4.9) [31] of R was used to conduct survival analysis.

Drug sensitivity and tumor mutation analysis

The R oncoPredict package (version 0.2) [32] was employed to examine the association between the chemotherapeutic response and immune grouping. Using the samples in the GDSC2 database as the training set, we predicted the drug sensitivity in different immune subgroups from two datasets (TCGA + GSE58812). Regarding copy number variation (CNV) and tumor mutation burden (TMB) analysis, Freqcnv = FALSE information of merged Masked Copy Number Segment data were extracted and organized into a standard format. The CNV analysis was conducted using the GISTIC_2.0 plugin from the GenePattern website. In this analysis, we selected single-nucleotide polymorphism (SNP) data calculated by the Varscan platform and used the R maftools package (version 2.1) [33] to obtain

the mutation differences between subtypes. The calculated TMB was statistically analyzed.

Single-cell data processing

TNBC single-cell data were mainly derived from the GEO database (GSE161529) and integrated using the Seurat R package (version 4.0.3) [34]. The DoubletFinder package (version 2.0.3) [35] was utilized to eliminate doublets by assuming a doublet formation rate of 4%. In total, a single-cell matrix of 22,836 (number of genes) * 36,704 (number of cells) was used for subsequent analysis. Batch effects were removed using the Harmony algorithm package (version 0.1.1) [36]. The Seurat R package [34] was utilized for normalization, dimension reduction, clustering, and identification of cluster-specific genes in the single-cell data. Visualization was performed using tSNE. The reported marker genes published in previous studies and the annotation results of the CellMarker 2.0 database [37] were combined for annotation of cell subsets. Deconvolution analysis was performed on the bulk RNA sequencing data using the BayesPrism package (version 2.0) [38].

Identification of phenotype-associated subpopulations using Scissor

The Scissor package (version 2.0.0) [39] was employed to identify cell subpopulations associated with immune grouping and measure the similarity between bulk data and single-cell data. Furthermore, the regression model of the matrix-phenotype correlation was optimized. Subsequently, the cell populations associated with phenotypes were determined through the penalty function and regularization rule of Scissor. In the case of the Cox regression model, Scissor+ cells were linked to the "hot" immune subtype, while Scissor- cells were linked to the "cold" immune subtype.

Cell line models and quantitative reverse transcription polymerase chain reaction (qRT-PCR)

Human mammary cell lines (MCF-10A, MDA-MB-231, HCC1806, and HCC1937) were purchased from ATCC. Cell culture, RNA extraction, and qPCR were performed as previously described according to standard protocols [40]. The primers used in our research are listed in Table S2.

Small interfering RNA (siRNA)-mediated lncRNA knockdown

The siRNAs against LINC01550 and negative control oligonucleotides were purchased from Sangon Biotech. Transfection of siRNA into TNBC cells was performed using the Lipofectamine® 3000 reagent (Invitrogen) according to the manufacturer's guidelines. The oligonucleotide sequences used in this study are listed in Table S2. qRT-PCR was performed to examine the knockdown efficiency.

Cell proliferation, apoptosis, and migration assays

All experiments were carried out 48 hours after cell transfection. Cell activity was determined using a CCK8 assay (Bimake). A colony formation assay was employed to assess the proliferative potential of breast cancer cells. Apoptosis was measured by flow cytometry. Briefly, the control and experimental groups were resuspended and stained using an Annexin V-FITC/PI kit (BioLegend). A flow cytometer (FACScan; BD Biosciences) was used to detect the fluorescence and apoptosis results. A wound-healing assay and transwell system were implemented for migration detection as previously described [33].

Statistical analysis

Experimental data analysis was performed using GraphPad Prism 9. All quantitative data were presented as the mean ± standard deviation and analyzed using Student's t-test or analysis of variance. All experiments were carried out independently in triplicate. Bioinformatic data handling, detailed statistical analyses, and graphic drawing were performed using R software (version 4.1.2). Statistical significance is represented as follows: no difference (ns): $P > 0.05$, *$P < 0.05$, **$P < 0.01$, ***$P < 0.001$.

Results

Recognition of immune infiltration consensus clusters of TNBC

A flow diagram (**Figure 1A**) shows the procedure of this bioinformatics research. Using gene signatures from 28 TILs and the ssGSEA method, we employed a consensus cluster to

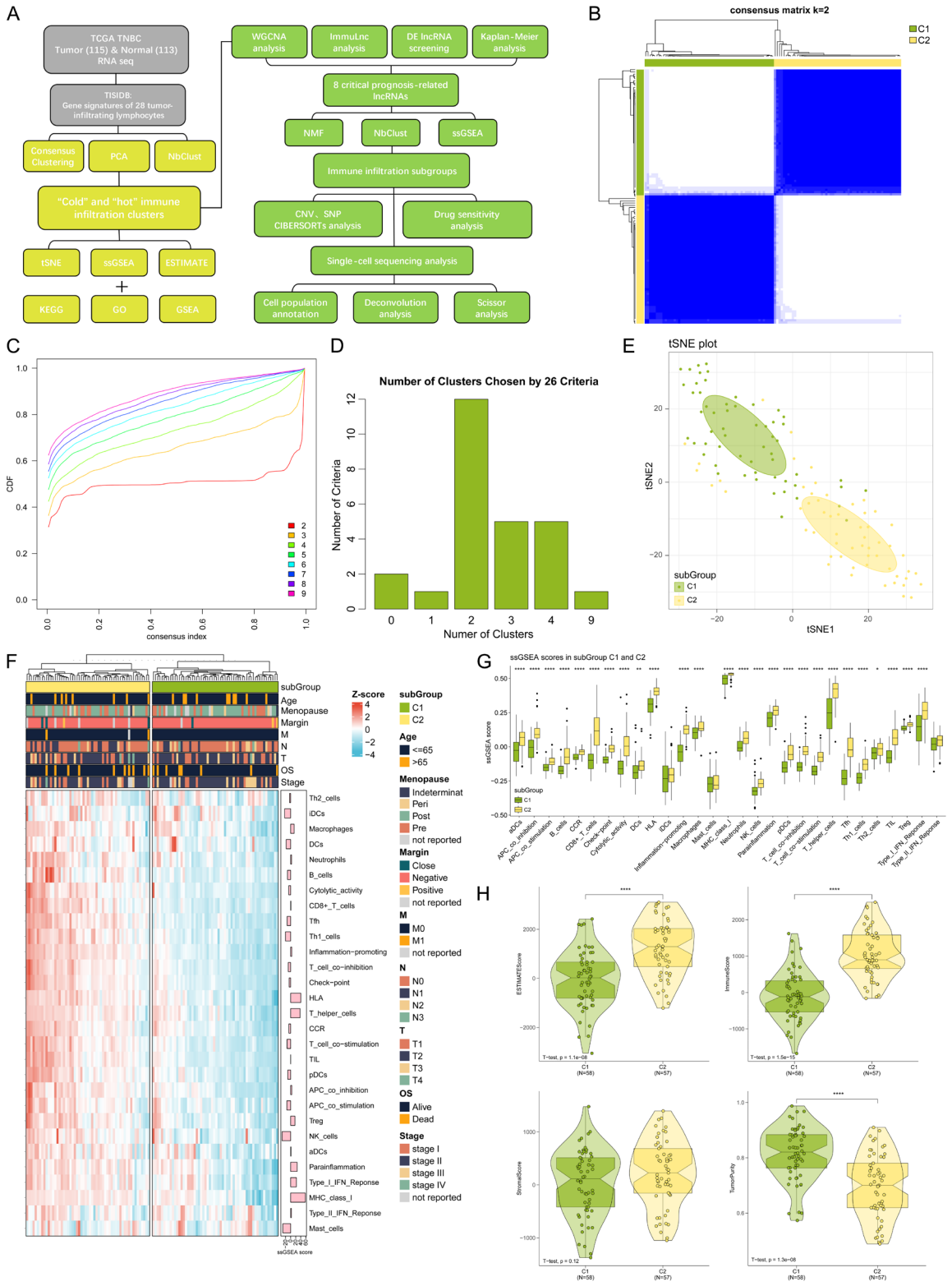

Figure 1. Identification of "immune-cold" and "immune-hot" triple-negative breast cancer (TNBC) tumor samples. A. Flowchart of bioinformatics study; B. Consensus score matrix of TNBC (cluster number k = 2); C. Cumulative distribution function curve of the consensus matrix indicated by colors (k = 2 to 9); D. Identification of the optimal number of clusters; E. t-Distributed stochastic neighbor embedding (tSNE) algorithm analysis of clusters; F. The infiltration abundance of immune cell subgroups evaluated by single-sample gene-set enrichment analysis (ssGSEA) for the C1

and C2 clusters; G. The ssGSEA scores of the C1 and C2 clusters; H. Comparison of immune scores, stromal scores, and tumor purity between the C1 and C2 clusters. Statistical analysis: no difference (blank): P > 0.05, *P < 0.05, **P < 0.01, ****P < 0.001.

categorize the immune infiltration clusters of TNBC samples. The determination of the optimal cluster number (k = 2) was based on the area under the cumulative distribution function curve in the consensus cluster and the proportion of the ambiguous clustering algorithm (**Figure 1B** and **1C**). NbClust testing was also conducted to confirm that the cluster number k = 2 (**Figure 1D**). The two primary consensus clusters were denoted as the "C1" and "C2" immune infiltrate groups. When subjected to dimensionality reduction using the tSNE method, C1 and C2 exhibited significant disparities in immune infiltration characteristics, as depicted in **Figure 1E**. C2 displayed a notably higher abundance of various immune cell subsets, as evidenced by the ssGSEA results (**Figure 1F** and **1G**). Consequently, we employed consensus k-mean clustering to classify C1 as immune-desert tumors and C2 as immune-inflamed tumors. Furthermore, the ESTIMATE method was performed to evaluate the tumor purity in each cluster to reflect the potential enrichment differences of immune cells between the two clusters (**Figure 1H**). Then, we employed five additional analytical algorithms, including quanTIseq, xCell, TIMER, MCP-counter, and EPIC, to validate the suitability and dependence of the clusters. This verification process was conducted independently of the ssGSEA analysis to ensure the reliability of the results (Figure S1). To summarize, we categorized the TNBC samples into two subgroups: immunogenic "hot" tumors and hypoimmunogenic "cold" tumors. The immune infiltration characteristics exhibited discernible disparities between these two groups.

Functional enrichment analysis of TNBC immune infiltrate clusters

Based on the aforementioned findings, we successfully categorized TNBC tumors into immune-cold (C1) and immune-hot (C2) clusters. We employed the limma package to further assess differential gene expression. A volcano plot and heatmap were used to effectively visualize the variations in mRNA expression between the C1 and C2 clusters. In total, we identified 547 upregulated and 6 downregulated mRNAs in the C2 cluster, with an absolute fold change value ≥ 1.5 and *p*-value < 0.05. Notably, the top upregulated genes (CXCL13, CXCL9, IDO1, CXCL10, MZB1, CCL19, and CCL5) encompassed specific chemokines, cytokines, and immune-related genes (**Figure 2A** and **2B**). The majority of DEGs in the C2 cluster were closely related to immune responses, including immunocyte activation, antigen presentation via MHC class II, immune response, and activity, which was indicated by GO analysis (**Figure 2C-E**). Next, the significant DEGs were subjected to KEGG pathway analysis, revealing the enrichment of pathways related to inflammation, immune response, and tumorigenesis. These pathways included antigen processing and presentation, Th1/2/17 cell differentiation, and interaction between cytokines and receptors (**Figure 2F**). The GSEA findings further supported the above results, indicating significant activation of immune and inflammatory pathways in the C2 cluster of TNBC (**Figures 2G** and S2). In summary, the functional enrichment analysis demonstrated that, as an immunogenic "hot" subgroup, the C2 cluster is featured with enhanced immune infiltration and immune recognition/activation.

Analysis of immune infiltration-related lncRNA modules

Immune infiltration-related lncRNA modules were identified using the WGCNA algorithm. Following the removal of outlier data and low-abundance genes, 218 lncRNA genes were included for further analysis (Table S3). A soft thresholding β was screened and set to 6, which was conducted using the PickSoftThreshold function, enabling the selection of an appropriate power value (**Figures 3A** and S3A). The cutreeStaticColor function of the WGCNA package was employed to reveal a total of eight modules (**Figure 3B**). When identifying modules relevant to the "hot" tumor subgroup, the module-trait relationship showed that the yellow module was the most relevant object (**Figures 3C** and S3B). The lncRNA genes contained in the yellow module are shown in Table S3. To further investigate the crucial lncRNAs related to immune infiltration, we conducted a

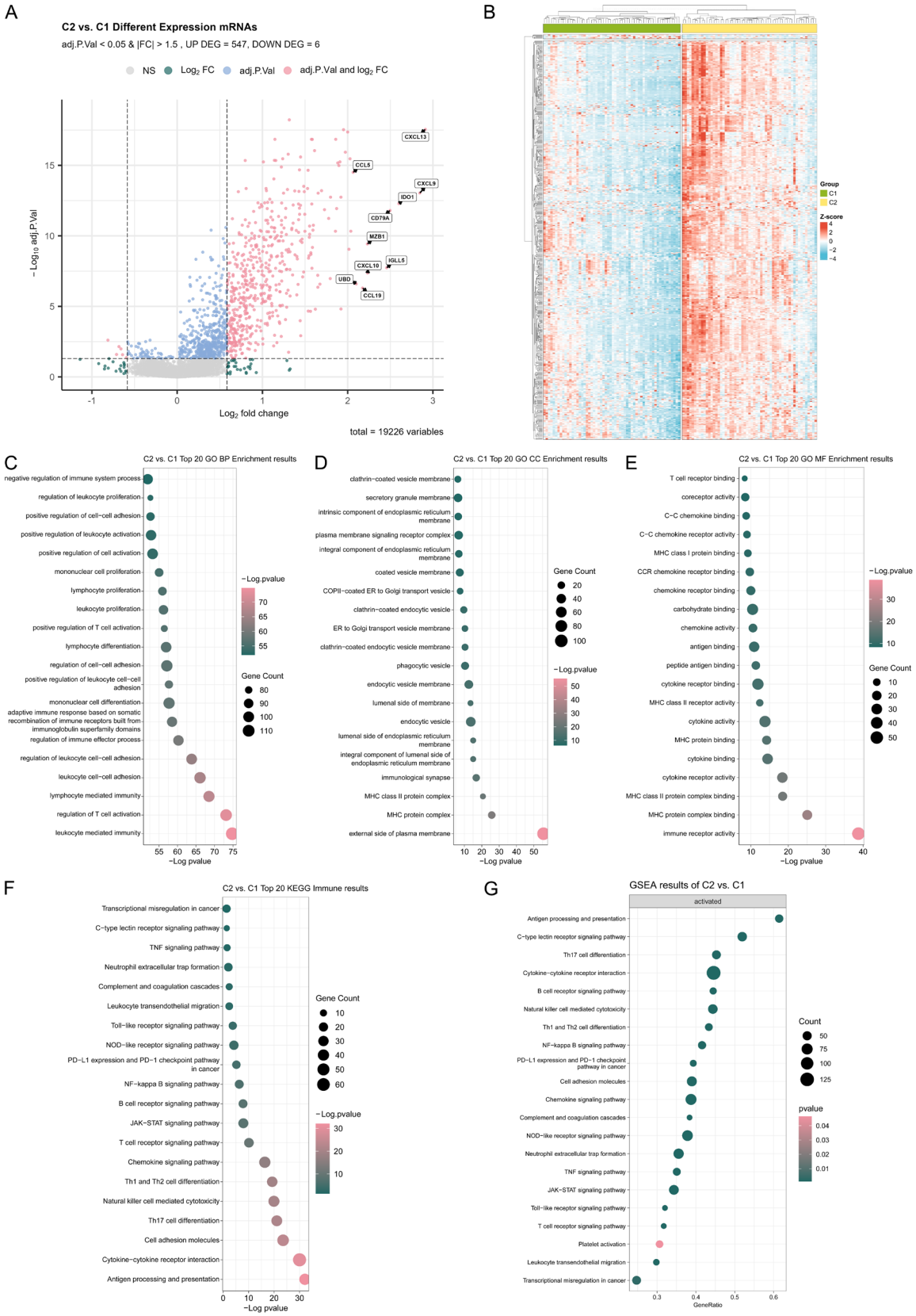

Figure 2. Functional analysis of differentially expressed genes in the “immune-cold” and “immune-hot” clusters. A, B. Volcano plot and heatmap of DEGs; C-E. Gene Ontology (GO) enrichment analysis results; F. Top 20 enriched Kyoto Encyclopedia of Genes and Genomes (KEGG) pathway items; G. Gene-set enrichment analysis (GSEA) bubble plot of differentially expressed genes (DEGs).

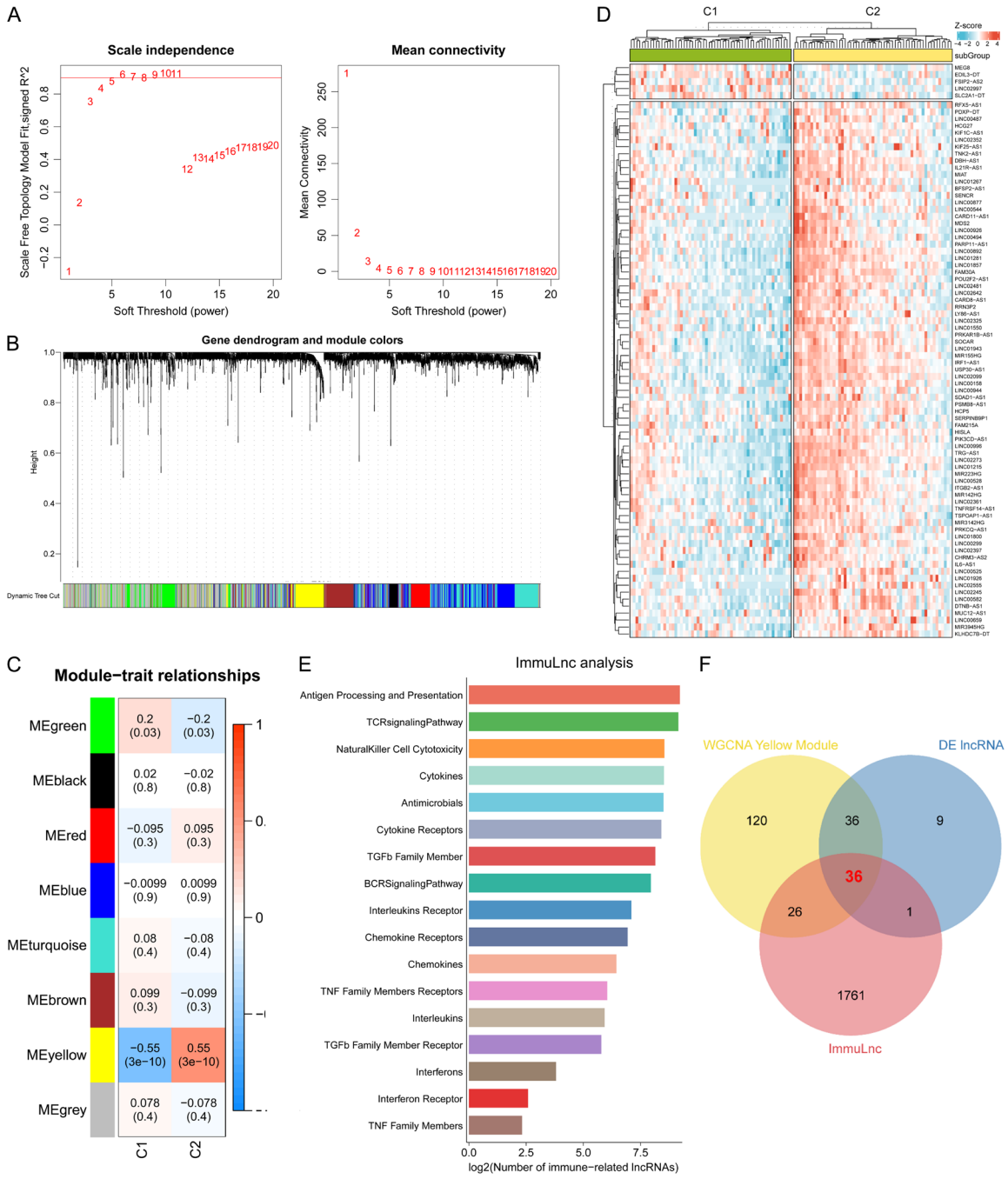

Figure 3. Identification of immune-related long noncoding RNAs (lncRNAs). A. The scale-free topology model fit (left) and the mean connectivity of the co-expression network (right) under different soft thresholds; B. Clustering dendrogram showing module membership; C. Module-trait relationships revealed lncRNAs correlated with immune infiltrate groups; D. Bidirectionally clustered heatmap displaying differential lncRNA expression between the C1 and C2 clusters; E. ImmLnc enrichment analysis of candidate immune-related pathways; F. Venn diagram of overlapping lncRNAs between weighted gene co-expression network analysis (WGCNA), ImmLnc, and DEG analyses.

differential analysis between the C1 and C2 clusters. The heat map and volcano map are shown in **Figures 3D** and S3C. A total of 82 lncRNAs exhibited differential expression levels between the C1 and C2 clusters, including 77 upregulated and 5 downregulated lncRNAs (Table S3). The ImmLnc integrated method was employed to identify lncRNAs that regulate

immune pathways of TNBC. Consequently, 1824 potential lncRNA regulatory factors that might be implicated in the modulation of immune-related pathway activity were identified. Notably, these lncRNAs were primarily associated with pathways such as the T cell receptor signaling pathway, antigen processing and presentation, and cytokines and cytokine receptors, as depicted in **Figure 3E**. The Venn diagram presented in **Figure 3F** provides a visual representation of the overlap between lncRNA genes identified through WGCNA analysis, DEG expression, and ImmLnc analysis. The resulting 36 lncRNA genes, obtained from this intersection, held potential as candidate molecules for the development of an immune-related prognosis model. Collectively, these lncRNAs are likely to exert significant influence on the regulation of immune infiltration within the immune microenvironment of TNBC.

Immune infiltration subtyping based on critical prognosis-related lncRNAs

The subsequent analysis focused on exploring the association between candidate lncRNAs and overall survival data from TCGA. We selected eight lncRNAs related to prognosis, as depicted in **Figure 4A**. Among these, LINC01550, LY86-AS1, LINC00877, and PIK3CD-AS1 were found to be linked to poor prognosis, while LINC00494, CHRM3-AS2, HCP5, and MIR155HG were identified as potential favorable prognosis predictors. Furthermore, an additional independent dataset (GSE58812) was employed as an independent validation dataset for survival analysis (**Figure 4B**). These eight prognosis-associated lncRNAs were utilized to establish immune infiltration subtyping.

Subsequently, TNBC patients were assigned into two subtypes (T1 and T2) in both TCGA dataset (**Figure 5A**) and the GSE58812 independent dataset (G1 and G2) (**Figure 5E**), based on the pivotal lncRNAs. The specific grouping information is listed in Table S4. In **Figure 5B** and **5F**, two predominant TCGA and independent dataset subgroups were confirmed by the non-negative matrix factorization method. The gene expression patterns of the core lncRNAs in different subgroups of both TCGA and the GSE58812 datasets were further compared, as shown in **Figure 5C** and **5G**. The results of dimensionality reduction analyses conducted using tSNE exhibited similar patterns to those of hierarchical clustering (**Figure 5D** and **5H**). The C1 and C2 tumor subtype clustering results of TCGA in **Figure 1** served as the basis, and we evaluated the initial distribution of samples in the T1 and T2 subgroups using a chi-squared test. The findings revealed that the T1 subtype predominantly consisted of primitive "cold" tumor samples, whereas the T2 subtype consisted of primitive "hot" tumor samples (**Figure 5I**). Additionally, the ssGSEA analysis indicated that both the T2 and G2 subgroups contained greater numbers of infiltrating immune cells (**Figure 5J** and **5K**). These findings suggest that the immune infiltration characteristics of the "hot" and "cold" subtypes exhibit significant differences according to critical prognosis-associated lncRNAs.

Differences in drug sensitivity, genome variation, and immune infiltration characteristics between immune infiltration subgroups

Subsequently, we compared the drug sensitivity between the "cold" and "hot" tumor subgroups for commonly used therapeutic cancer drugs. The findings depicted in **Figure 6A** demonstrate notable statistical disparities for four frequently employed drugs - palbociclib, mitoxantrone, ribociclib, and sorafenib. The half-maximal inhibitory concentration (IC_{50}) values observed in the "hot" subgroup (T2) were significantly lower than those in the "cold" group (T1), suggesting that TNBC patients belonging to the "hot" tumor subgroup may potentially experience clinical benefits from these anticancer drugs. A similar finding was further confirmed in the GSE58812 dataset (**Figure 6B**).

Previous studies have established a correlation between CNVs, the TMB, and the responsiveness of TNBC to immunotherapy and chemotherapy drugs. Therefore, we investigated the genomic variation characteristics of the two immune subgroups. The representation of CNVs in TCGA samples (**Figure 6H-J**) revealed minor discrepancies. **Figure 6C** and **6D** indicate a lack of noticeable disparities in CNVs and deletion events. **Figure 6F** presents a waterfall plot of the top 20 somatic SNPs in the subgroups. A higher TMB degree corresponds to a more favorable survival outcome

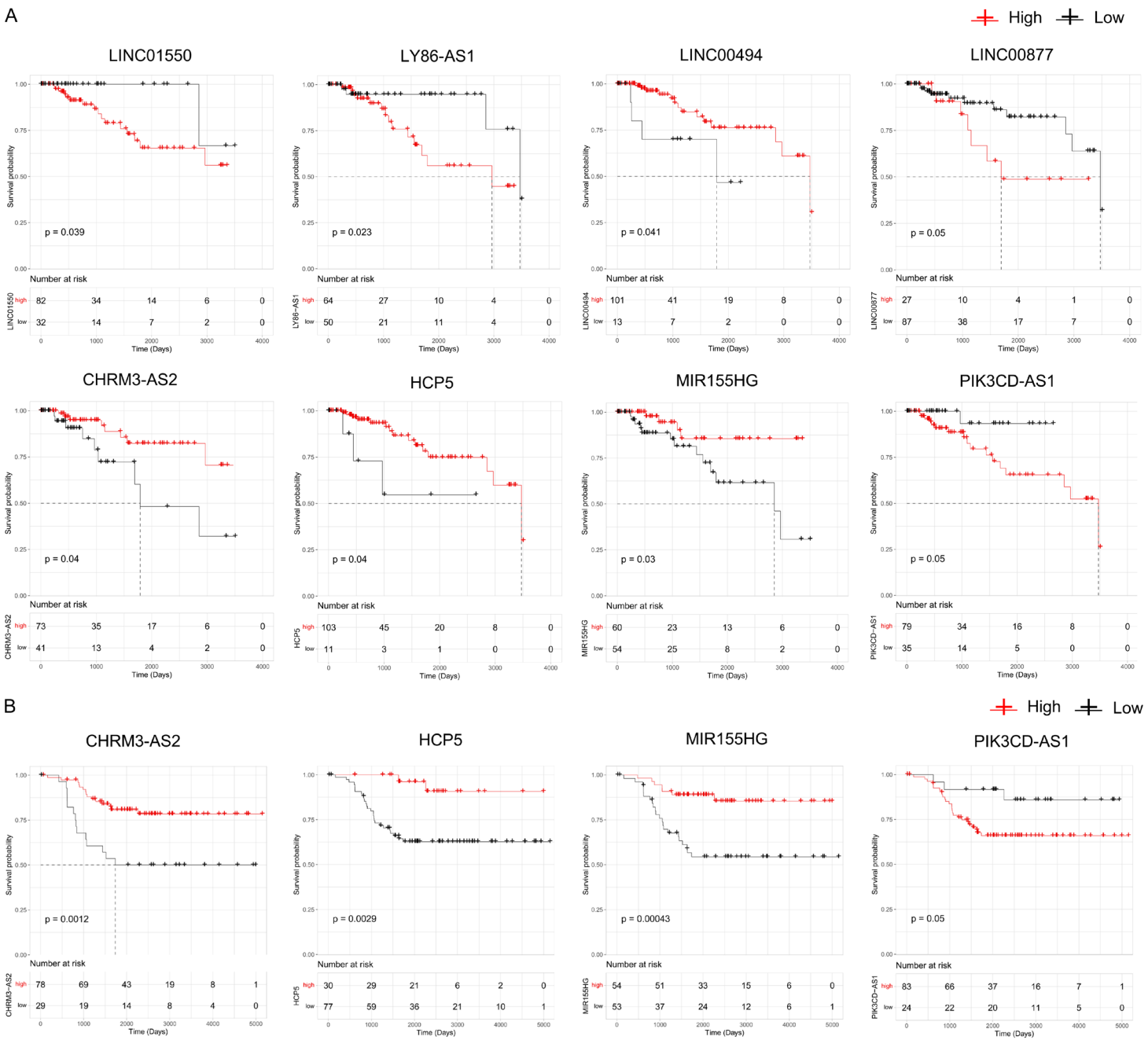
A
High
Low
LINC01550
p = 0.039
LY86-AS1
p = 0.023
LINC00494
p = 0.041
LINC00877
p = 0.05
CHRM3-AS2
p = 0.04
HCP5
p = 0.04
MIR155HG
p = 0.03
PIK3CD-AS1
p = 0.05
Survival probability
Number at risk
Time (Days)
B
High
Low
CHRM3-AS2
p = 0.0012
HCP5
p = 0.0029
MIR155HG
p = 0.00043
PIK3CD-AS1
p = 0.05

Figure 4. Kaplan-Meier plots of significant prognosis-associated lncRNAs from The Cancer Genome Atlas (TCGA) (A) and the GSE58812 (B) databases.

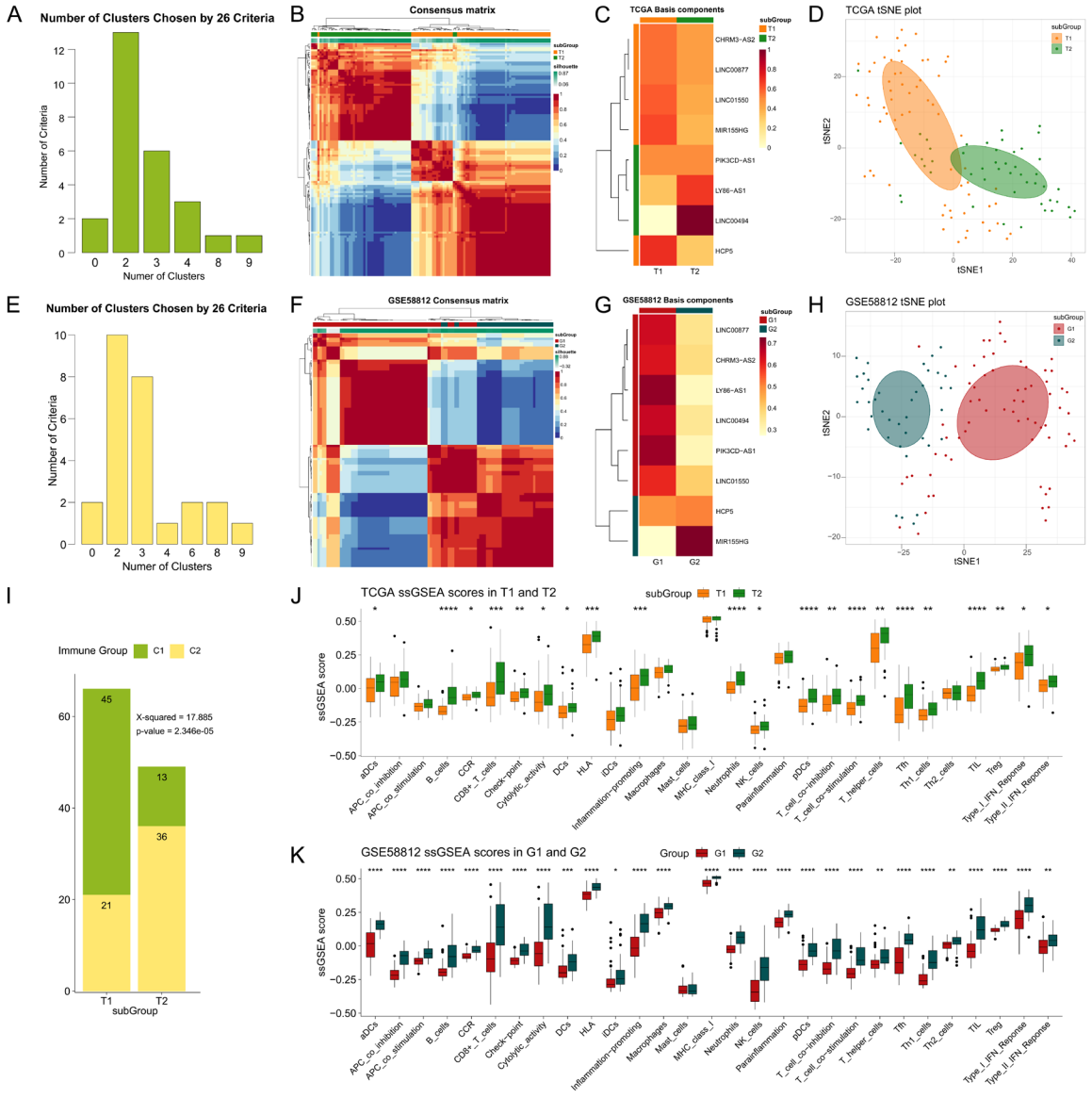

Figure 5. "Cold" and "hot" tumor typing of TNBC based on core lncRNAs. (A and E) Consensus clustering by selecting k = 2 as the optimal choice to determine the clustering number of TCGA dataset (A) and the GSE58812 dataset (E); (B and F) Hierarchical clustering of the consensus matrix in TCGA (B) and the GSE58812 (F) datasets; (C and G) Expression pattern heatmaps of core lncRNAs in different immune infiltration groups of TCGA dataset (C) and the independent validation set GSE58812 (G); (D and H) Dimensionality reduction plot of TNBC samples of TCGA (D) and GSE58812 (H) data; (I) A chi-square test of independence showed a significant association between distinct clusters based on mRNA and lncRNA; (J and K) ssGSEA enrichment score difference in "cold" and "hot" subgroups of TCGA (J) and the GSE58812 (K) datasets. Statistical analysis: no difference (blank): P > 0.05, *P < 0.05, **P < 0.01, ***P or ****P < 0.001.

(**Figure 6E**). No significant differences in TMB levels were determined **Figure 6G**. Consequently, this finding suggests that CNVs and TMB may not be the main factors contributing to significant variations in drug responses between the T1 and T2 groups.

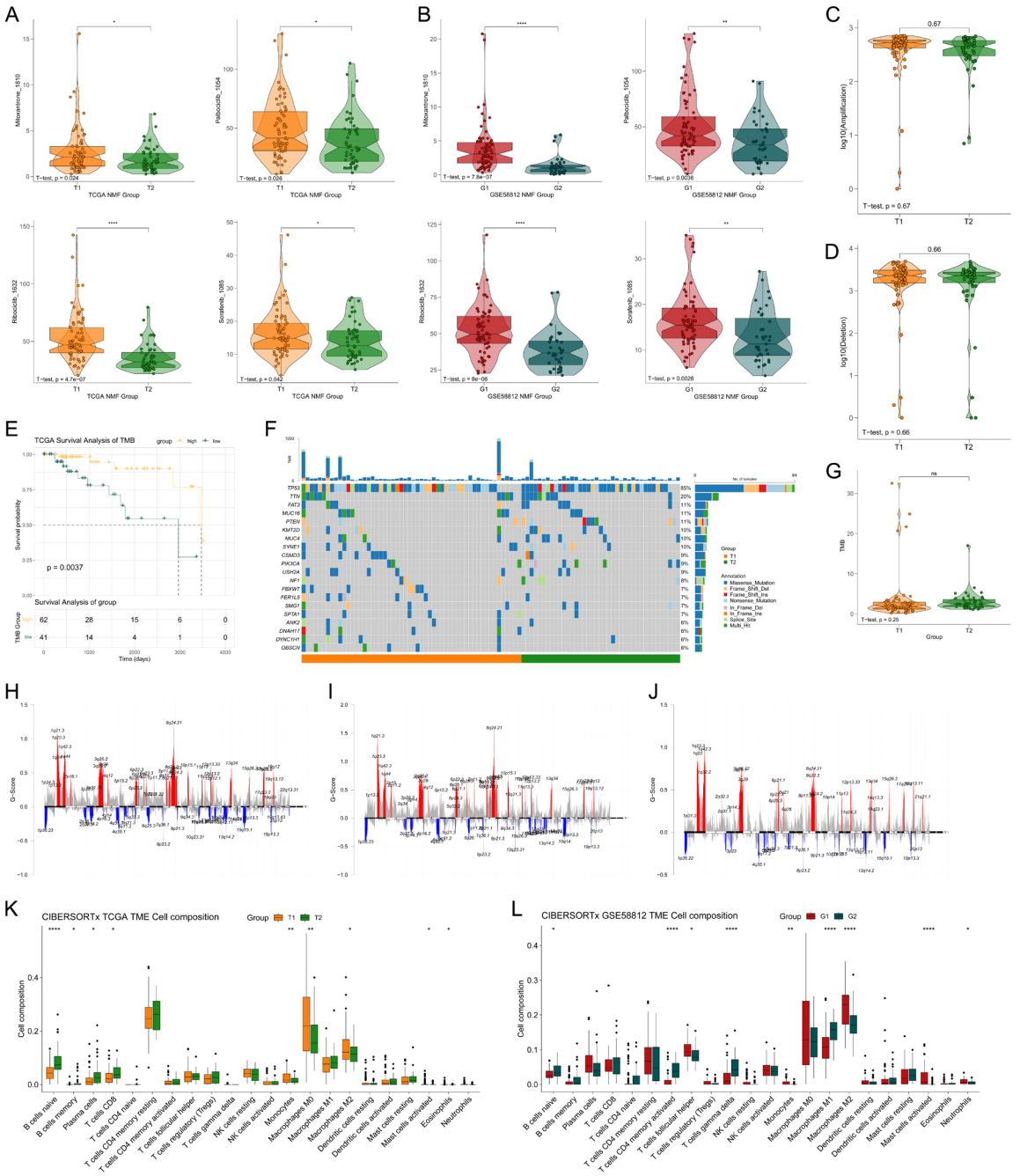

Figure 6. Analysis of drug sensitivity, the genome, and immune infiltration. (A and B) Drug sensitivity difference for anti-tumor agents in TCGA (A) and the GSE58812 (B) TNBC datasets; (C and D) Statistical analysis of copy number amplification events (C) and deletion events (D) between the "cold" and "hot" subgroups in TCGA dataset; (E) Survival analysis based on the tumor mutation burden (TMB) of TCGA samples; (F) Waterfall plots of the top single-nucleotide polymorphism genes in the T1 and T2 subgroups; (G) Statistical difference analysis of TMB between the T1 and T2 subgroups; (H-J) Copy number variation analysis of all TNBC samples (H), the T1 subgroup (I), and the T2 subgroup (J); (K and L) Deconvolution analysis of the infiltrating immune cell proportion in TCGA (K) and the GSE58812 (L) datasets. Statistical analysis: no difference (blank or ns): P > 0.05, *P < 0.05, **P < 0.01, ***P or ****P < 0.001.

The TNBC datasets underwent deconvolution analysis using the CIBERSORTx algorithm. Statistical analyses indicated that the varying responses of TNBC in different immune infiltration subgroups to clinical drug treatment may be attributable to discrepancies in the propor-

tions of immune cells, particularly B lymphocytes or macrophages, within the tumor immune microenvironment (**Figure 6K** and **6L**). Furthermore, we conducted a correlation analysis to examine the relationship among eight core lncRNAs, immune checkpoint markers, and immune cell infiltration in the validation set of the GSE58812 and TCGA databases (Figure S4). T lymphocytes, B lymphocytes, and macrophages exhibited a significant positive correlation with the expression of core lncRNAs in the tumor microenvironment.

Determination of the cellular composition of different TNBC immune types by single-cell sequencing analysis

It was hypothesized that the disparities in drug sensitivity of different immune subgroups might be attributable to variations in the cellular composition within the tumor microenvironment. Initially, single-cell data preprocessing was conducted on the eight TNBC samples from the GSE161529 dataset to eliminate abnormal cell components and genes that were irrelevant to subsequent analyses. A single-cell matrix consisting of 22,836 genes and 36,704 cells was obtained to ensure quality control and remove batch effects between datasets. The pre- and post-integration single-cell data are shown in Figure S5. **Figure 7A** presents the tSNE dimensionality reduction clustering visualization after batch effects were eliminated. Cell clustering was conducted on the dimension-reduced data using single-cell marker genes identified by cell type (**Figure 7B**). Table S1 lists the marker genes associated with different cell types. In **Figure 7C**, 15 distinct cell populations are identified and distinguished using various color markers. Following the cell annotation analysis of the TNBC single-cell data, we performed deconvolution analysis on bulk RNA sequencing data of TCGA and the GSE58812 datasets using the BayesPrism package to determine the cellular composition. Based on the findings derived from **Figure 7D** and **7F**, it was observed that endothelial cells and cycling cells were the predominant types in both datasets, followed by fibroblasts and neutrophils. **Figure 7E** and **7G** indicate a noteworthy increase in B lymphocytes and plasmacytoid dendritic cells (pDCs), while a noticeable decrease in epithelial cells and cycling cells was observed within the "hot" tumor subgroup. Consequently, it is postulated that alterations in the proportions of epithelial cells, cycling cells, B cells, and pDC cells could exert a substantial influence on the tumor microenvironment and potentially influence differences in the drug response between the "cold" and "hot" TNBC tumor subgroups.

Identification of immune grouping-associated cell subpopulations using the Scissor algorithm

Immune-phenotype analysis was employed using the Scissor algorithm of R. The Scissor+ cell subset demonstrated a significant correlation with the "cold" clusters (T1 and G1), while the Scissor- cell subset was related to "hot" clusters (T2 and G2). **Figure 8A** and **8C** illustrate the distribution of Scissor (+/-) cells in dimensionality reduction cluster maps for the GSE58812 and TCGA datasets. The proportions of Scissor (+/-) cells within different subsets are illustrated in **Figure 8B** and **8D**. The results indicate that in both TCGA and the validation set, Scissor analysis produced a similar conclusion, where most B cells and pDCs were identified as Scissor- cells. These cells were more closely associated with the "hot" immune infiltrating subtype. Next, we performed an analysis to determine the correlations among four specific anti-tumor drugs (palbociclib, ribociclib, mitoxantrone, and sorafenib) and the proportions of B lymphocytes and pDCs in both datasets. The proportions of B cells and pDCs exhibited significantly positive correlations with sensitivity to the aforementioned anti-tumor drugs in TNBC (**Figure 8E** and **8F**). Hence, we speculate that variations in the proportions of B cells and pDCs may be a primary reason for the notable disparities observed in drug responses between different immune subsets of TNBC.

LINC01550 affects the malignant phenotype of TNBC

Based on the survival analysis presented in **Figure 4A**, we further validated the relative expression levels of four poor prognosis-associated lncRNAs in normal and breast cancer cell lines using RT-qPCR. LINC01550 expression was higher in the three types of TNBC cells compared with that in MCF-10A cells, as illustrated in **Figure 9A**, suggesting that LINC01550 may serve as a tumor-specific gene, exerting regulatory effects on the biological behavior of TNBC. Consequently, two LINC01550 siRNAs were synthesized, and their efficiency was confirmed in MDA-MB-231

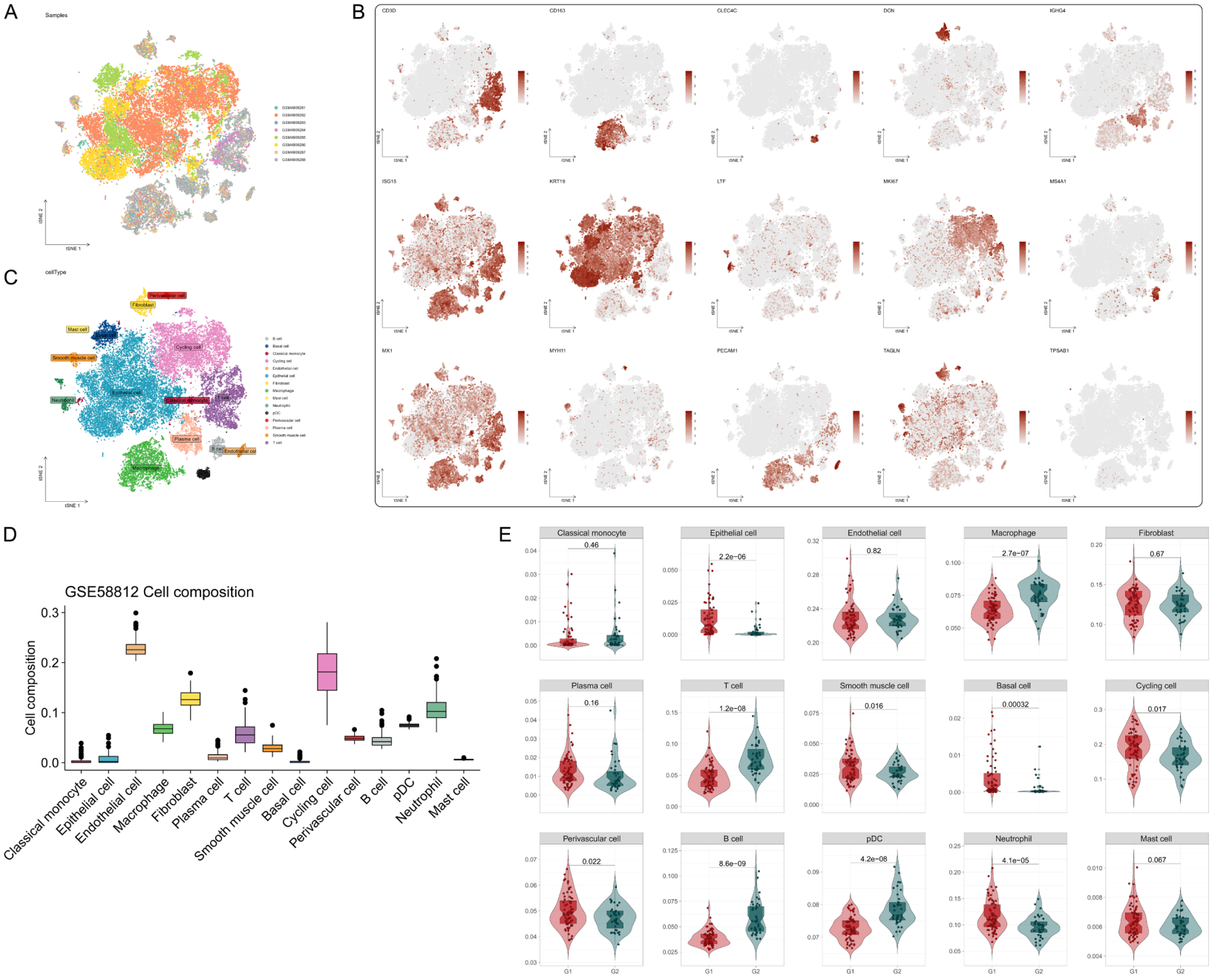
A
Samples
B
CD3D
CD163
CLEC4C
DCN
IGHG4
ISG15
KRT19
LTF
MKI67
MS4A1
MX1
MYH11
PECAM1
TAGLN
TPSAB1
C
cellType
Perivascular cell
Fibroblast
Mast cell
Cycling cell
Smooth muscle cell
Epithelial cell
Neutrophil
Plasma cell
B cell
Endothelial cell
Macrophage
T cell
D
GSE58812 Cell composition
Cell composition
Classical monocyte
Epithelial cell
Endothelial cell
Macrophage
Fibroblast
Plasma cell
T cell
Smooth muscle cell
Basal cell
Cycling cell
Perivascular cell
B cell
pDC
Neutrophil
Mast cell
E
Classical monocyte
0.46
Epithelial cell
2.2e−06
Endothelial cell
0.82
Macrophage
2.7e−07
Fibroblast
0.67
Plasma cell
0.16
T cell
1.2e−08
Smooth muscle cell
0.016
Basal cell
0.00032
Cycling cell
0.017
Perivascular cell
0.022
B cell
8.6e−09
pDC
4.2e−08
Neutrophil
4.1e−05
Mast cell
0.067
G1
G2

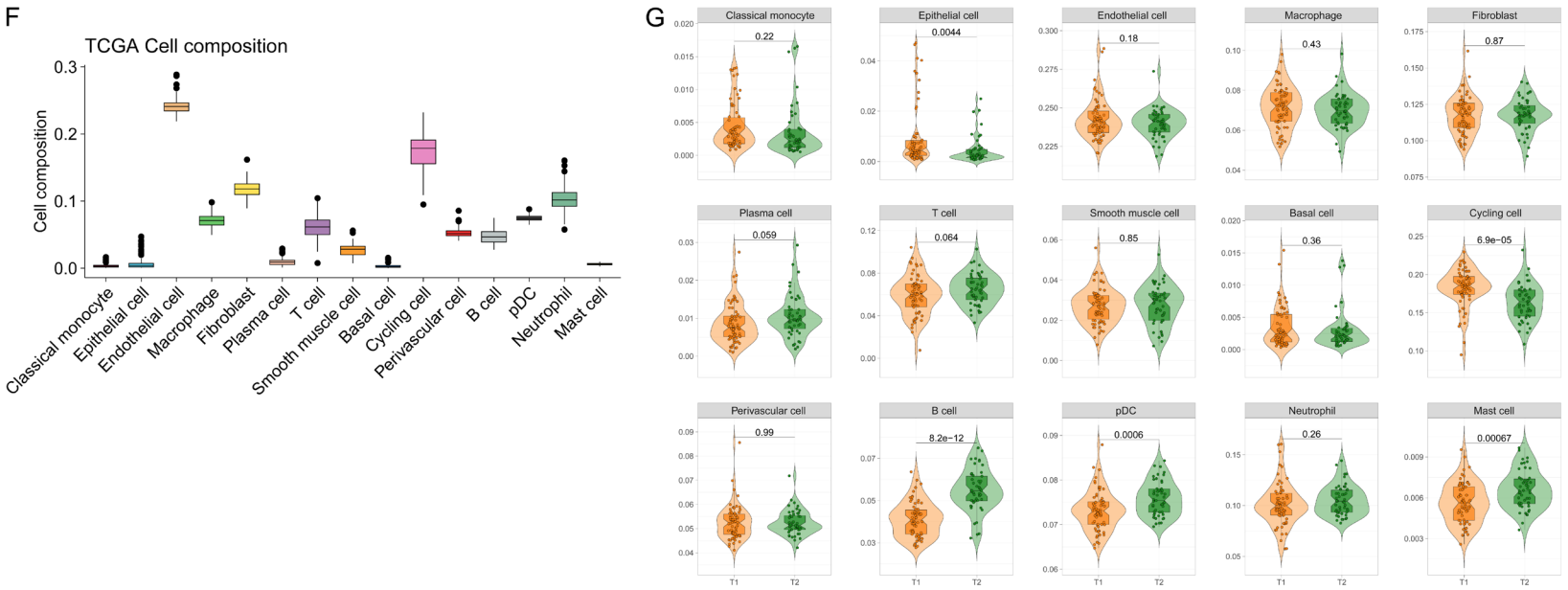

Figure 7. Single-cell data analysis of TNBC. A. tSNE dimensionality reduction clustering of single-cell data in the GSE161529 dataset; B. Gene expression-based clustering of single cells by tSNE; C. tSNE plot annotated by cell type; D. Cell composition deconvolution analysis of GSE58812 bulk RNA sequencing data; E. Differentiation analysis of cell composition between the G1 and G2 clusters; F. Cell composition deconvolution analysis of TCGA bulk RNA sequencing data; G. Differentiation analysis of cell composition compared between the T1 and T2 subgroups.

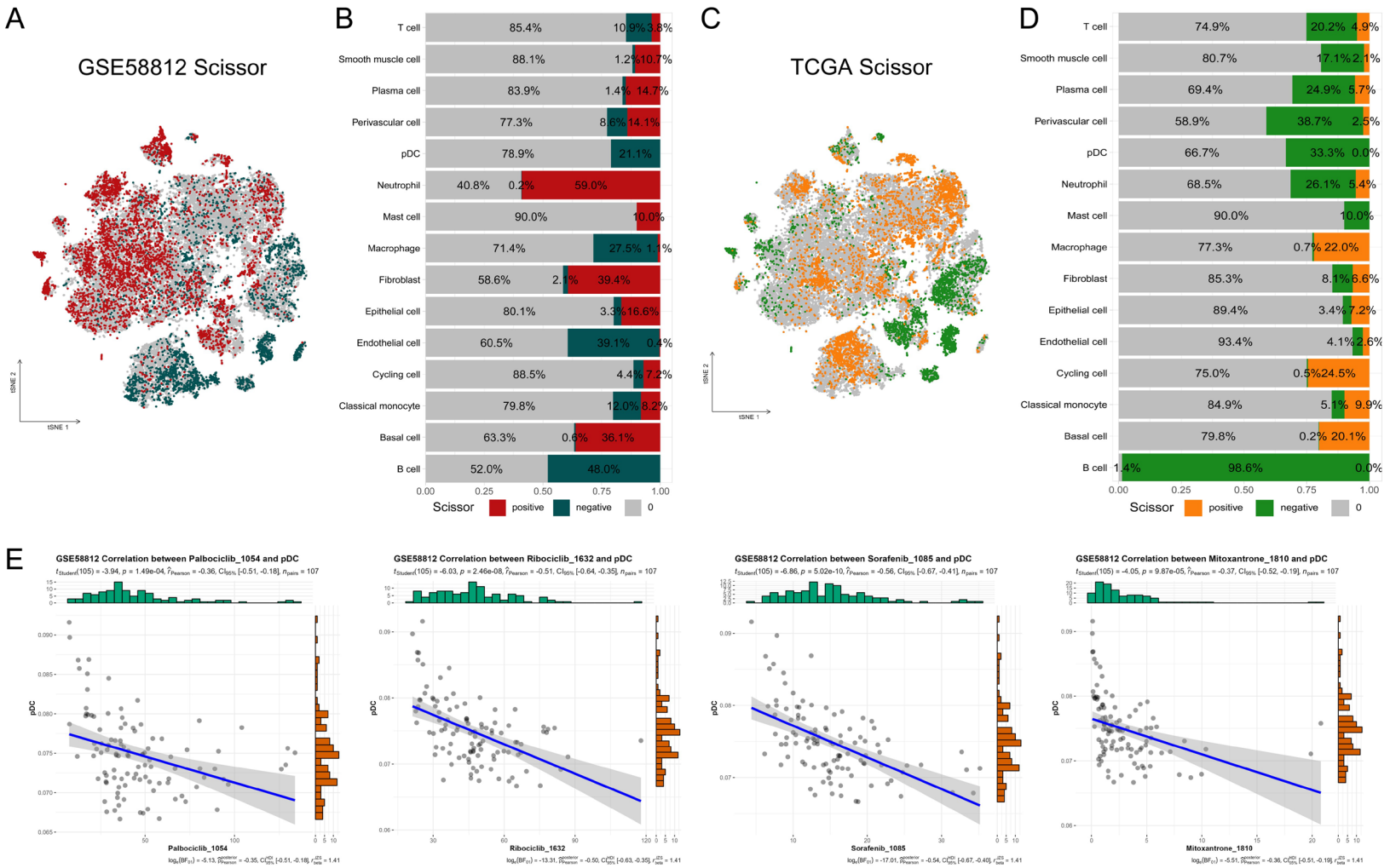
A
GSE58812 Scissor
tSNE 2
tSNE 1
B
T cell 85.4% 10.9% 3.8%
Smooth muscle cell 88.1% 1.2% 10.7%
Plasma cell 83.9% 1.4% 14.7%
Perivascular cell 77.3% 8.6% 14.1%
pDC 78.9% 21.1%
Neutrophil 40.8% 0.2% 59.0%
Mast cell 90.0% 10.0%
Macrophage 71.4% 27.5% 1.1%
Fibroblast 58.6% 2.1% 39.4%
Epithelial cell 80.1% 3.3% 16.6%
Endothelial cell 60.5% 39.1% 0.4%
Cycling cell 88.5% 4.4% 7.2%
Classical monocyte 79.8% 12.0% 8.2%
Basal cell 63.3% 0.6% 36.1%
B cell 52.0% 48.0%
0.00 0.25 0.50 0.75 1.00
Scissor positive negative 0
C
TCGA Scissor
tSNE 2
tSNE 1
D
T cell 74.9% 20.2% 4.9%
Smooth muscle cell 80.7% 17.1% 2.1%
Plasma cell 69.4% 24.9% 5.7%
Perivascular cell 58.9% 38.7% 2.5%
pDC 66.7% 33.3% 0.0%
Neutrophil 68.5% 26.1% 5.4%
Mast cell 90.0% 10.0%
Macrophage 77.3% 0.7% 22.0%
Fibroblast 85.3% 8.1% 6.6%
Epithelial cell 89.4% 3.4% 7.2%
Endothelial cell 93.4% 4.1% 2.6%
Cycling cell 75.0% 0.5% 24.5%
Classical monocyte 84.9% 5.1% 9.9%
Basal cell 79.8% 0.2% 20.1%
B cell 1.4% 98.6% 0.0%
0.00 0.25 0.50 0.75 1.00
Scissor positive negative 0
E
GSE58812 Correlation between Palbociclib_1054 and pDC
GSE58812 Correlation between Ribociclib_1632 and pDC
GSE58812 Correlation between Sorafenib_1085 and pDC
GSE58812 Correlation between Mitoxantrone_1810 and pDC
pDC
Palbociclib_1054
Ribociclib_1632
Sorafenib_1085
Mitoxantrone_1810

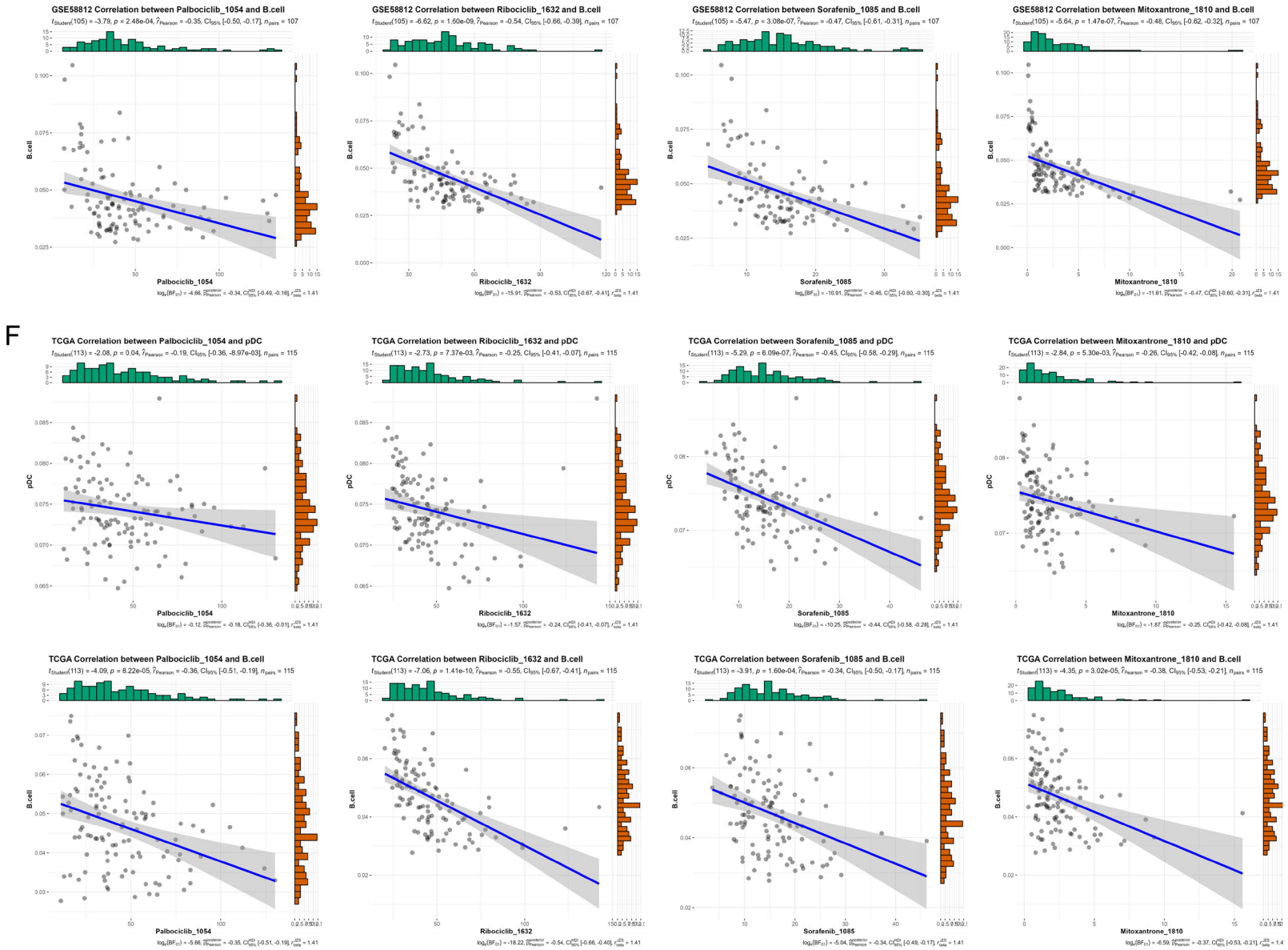

Figure 8. Identification of immune-grouping-associated cell subpopulations and correlation analysis of drug sensitivity. (A and C) Visual distribution of Scissor (+/-) cells in the dimensionality reduction diagram of bulk sequencing data in the GSE58812 (A) and TCGA (C) datasets; (B and D) Proportion of Scissor (+/-) cells of different types in the GSE58812 (B) and TCGA datasets (D); (E and F) Correlation analysis of proportions of B cells (E) and plasmacytoid dendritic cells (pDCs) (F) and IC_{50} values of drugs in the GSE58812 and TCGA datasets.

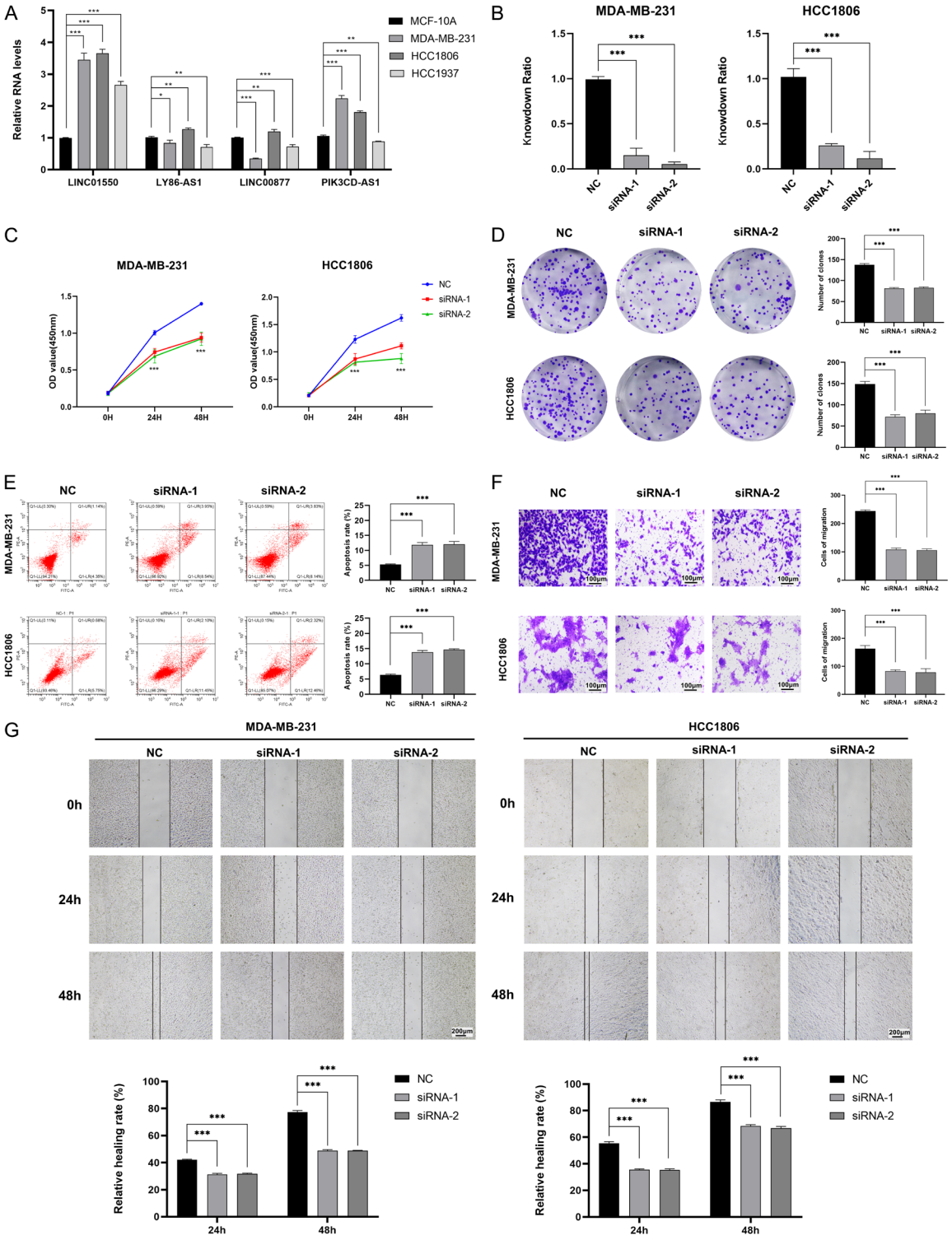

Figure 9. LINC01550 induces the proliferation, survival, and migration of TNBC. A. Relative RNA levels of four poor prognosis-related lncRNAs in normal and TNBC cell lines; B. Verification of small interfering RNA (siRNA)-mediated LINC01550 knockdown efficiency in TNBC cells; C. CCK8 assay of cells transfected with negative control (NC) siRNA and LINC01550 siRNAs; D. The cell proliferation abilities under NC/LINC01550 siRNA treatment were assessed using a cloning formation assay; E. Quantification of the apoptosis rate by flow cytometric analysis after transfection with siRNAs; F. Transwell migration assay; G. The wound-healing rate of NC and LINC01550-knockdown cells was analyzed using a cell wound-healing assay. No significant difference (ns): $P > 0.05$, *$P < 0.05$, **$P < 0.01$, ***$P < 0.001$.

and HCC1806 cells (**Figure 9B**). A CCK8 assay demonstrated that LINC01550 inhibition hindered the growth of TNBC cells (**Figure 9C**), and a colony formation assay demonstrated that inhibition of LINC01550 expression affected the colony formation abilities of TNBC cells (**Figure 9D**). Flow cytometry showed that after treatment with LINC01550 siRNAs, the numbers of late and especially early apoptotic cells significantly increased (**Figure 9E**). Furthermore, as shown in **Figure 9F** and **9G**, a transwell migration assay and wound-healing test revealed significant inhibition of tumor migration upon the suppression of LINC01550 expression in TNBC cells. These in vitro findings provide evidence that LINC01550, as a significant DEG, might promote the proliferation, migration, and apoptosis abilities of TNBC.

Discussion

TNBC is a type of breast cancer with refractory characteristics and high malignancy. Previous studies have identified two main clusters of TNBC subtypes, immune-desert (cold) and immune-inflamed (hot) [41]. Tumors with an immune-desert phenotype typically exhibit reduced responsiveness to immune therapy and poor clinical outcomes, whereas the immune-inflamed phenotype exhibits substantial infiltration of both adaptive and innate immune cells, with a better prognosis. The microenvironment of immune-inflamed tumors is mainly composed of natural killer (NK) cells, CD8+ T cells, and M1 macrophages. NK cells are cytotoxic lymphocytes and an important component of the innate immune response. CD8+ T cells are the main cytotoxic lymphocytes in the tumor microenvironment. M1 macrophages have pro-inflammatory effects, can activate immune responses and inhibit tumor development. In contrast, the immune-desert tumor microenvironment is formed by M2 macrophages, Foxp3+ regulatory T lymphocytes, and myeloid suppressive cells [42]. To perform a more accurate evaluation of the immune microenvironment of TNBC, we employed the ssGSEA method to analyze the TIL enrichment fraction in TCGA-TNBC cohort. We proposed a novel approach to categorize TNBC into immune-desert and immune-inflamed subgroups. Additionally, database exploration using the ESTIMATE and TIMER algorithms was performed to uncover the comprehensive landscape of the immune microenvironment. Notably, significant differences in the infiltration of core immune cells, including CD4+/CD8+ T lymphocytes, macrophages, B lymphocytes, and dendritic cells, were observed between the two clusters. KEGG analysis and GSEA revealed substantial enrichment of diverse classical signaling pathways related to immune, inflammatory, cytokine-mediated, and chemokine signaling in the DEGs. Our research enhances the understanding of the immune microenvironment in TNBC and may offer valuable insights for the clinical stratification of patients.

In the past decade, extensive transcriptomic investigations demonstrated that approximately 80% of human transcripts are composed of noncoding genes, such as lncRNAs [43]. An increasing number of studies have elucidated the significant contributions of lncRNAs to tumor progression, encompassing pivotal roles in proliferation, angiogenesis, migration, and metastasis [44-47]. Recent investigations have also indicated that some lncRNAs play crucial roles in regulating diverse functions within the immune system. Consequently, lncRNAs may offer valuable insights for optimizing cancer treatment decisions in clinical settings. For instance, it has been observed that the overexpression of lncRNA NKILA in tumor-specific cytotoxic T lymphocytes (CTLs) was associated with T-cell apoptosis and reduced survival. By downregulating NKILA expression in CTLs, enhanced infiltration of CTLs occurs in breast tumors, consequently leading to activation-induced death of T cells [48]. The latent roles of the lncRNA risk score model as a predictive indicator in cancer therapy have been extensively investigated, specifically in hepatocellular carcinoma, gastric cancer, and bladder cancer [49-51]. However, investigation into the potential contribution of the immune-related lncRNA signature in TNBC remains inadequate. Therefore, we employed the WGCNA method to identify the lncRNA module that was most closely associated with immune infiltration grouping. Kaplan-Meier analysis facilitated the identification of eight prognostic lncRNA molecules: LINC01550, LY86-AS1, LINC00494, LINC00877, CHRM3-AS2, HCP5, MIR155HG, and PIK3CD-AS1. These lncRNAs were incorporated into the development of an immune predictive risk

score model. The results presented in our study provide compelling evidence of a significant association between the crucial lncRNAs and immune cell infiltration of TNBC, including CD8+ T cells, macrophages, and neutrophils. Among these eight prognostic-related lncRNAs, we found that LINC01550 is highly expressed in TNBC and promotes malignant behavior in tumors. This discovery enhances the understanding of the novel function of LINC01550.

Additionally, our study revealed statistically significant differences in the efficacy of the four anti-tumor drugs between the immune-desert and immune-inflamed subgroups. The four anti-tumor drugs include two CDK4/6 inhibitors: palbociclib and ribociclib, a targeted drug: sorafenib, and a chemotherapy drug: mitoxantrone. The IC_{50} values of the immune-inflamed subgroup were significantly lower than those of the immune-desert subgroup, suggesting that TNBC patients in the immune "hot" group are more sensitive to the four anti-tumor drugs. Palbociclib and ribociclib, as third-generation CDK4/6 inhibitors, have been granted Food and Drug Administration approval for advanced breast cancer treatment in conjunction with HR+ HER2- breast cancer [52-54]. Similarly, CDK4/6 inhibitors combined with PI3Kα inhibitors enhance immunogenic cell death in TNBC by augmenting the infiltration and activation of CTLs within the tumor microenvironment and reducing the infiltration of myeloid-derived suppressor cells [55]. Mitoxantrone, as a potent topoisomerase II inhibitor, effectively binds to DNA and inhibits replication, resulting in the induction of double-strand breaks and disruption of RNA synthesis [56]. Mitoxantrone is commonly used in the treatment of breast cancer, leukemia, and non-Hodgkin lymphoma [57]. Previous research has demonstrated that mitoxantrone can induce immunogenic cancer cell death and elicit strong anticancer immune responses [58]. Sorafenib, a novel multi-kinase inhibitor, specifically targets tumor proliferation and angiogenesis. It has obtained approval for treatment of advanced renal cell cancer and hepatocellular carcinoma, and it is presently under evaluation for other malignancies [59]. The integration of chemotherapy with immunotherapy has proven to be a successful approach to cancer treatment. Consequently, our discoveries offer novel insights into the management of patients with TNBC.

The significance of TILs in immunosurveillance and the anti-tumor immune response has been established. TILs are strongly correlated with tumor progression, recurrence, chemotherapy response, and survival outcomes [60, 61]. The literature demonstrates that activation of tumor-infiltrating B lymphocytes (TIL-Bs) enhances the anti-tumor activity and regulation of immune checkpoints in a TNBC animal model [62]. Moreover, among the mechanisms of tumor cell killing, the density of TIL-Bs and the efficacy of chemotherapeutic agents mutually induce and promote each other, synergistically accelerating tumor regression in human and mouse tumor models [63]. An in vivo experiment confirmed that the triple therapy regimen of low-dose chemotherapy, oncolytic virotherapy, and immune checkpoint inhibitors could effectively enhance TIL-Bs and promote TNBC killing, which reflects the importance of TIL-Bs as drivers of anti-tumor immunity [64]. Nonetheless, the precise contribution of pDCs to tumor immunity remains uncertain. In the context of anti-tumor cellular immunity, pDCs have been recognized as effector cells in some studies. The activation of pDCs leads to direct tumor cell killing through mechanisms dependent on TRAIL and Granzyme B, ultimately resulting in tumor regression [65, 66]. Alternatively, tumor-infiltrated pDCs could synergize with conventional DCs to enhance the induction of the CD8+ T cell-mediated anti-tumor immune response, thereby improving the prognosis of patients [67]. In this study, deconvolution and Scissor analysis were performed to determine the lymphocyte composition in different immune infiltration subgroups. We observed a marked increase in the proportion of B lymphocytes and pDCs within the "hot" immune subgroup, which is strongly associated with favorable drug responsiveness to palbociclib, ribociclib, mitoxantrone, and sorafenib. The result suggests that the disparity in B cell and pDC infiltration between the immune-desert and immune-inflamed subgroups may be the primary contributing factor for the sensitivity to anti-tumor drugs.

Although our research has taken a new step in the immunophenotyping of TNBC, there are inevitably certain limitations that warrant

acknowledgment. First, the development and verification of the eight-lncRNA signature exclusively depended on TCGA and the GSE-58812 datasets. It is necessary to obtain additional appropriate external datasets to validate our lncRNA model. Second, the design of our study was retrospective, and it is imperative to conduct prospective studies for further validation of the universality of the lncRNA signature. Moreover, the suitability of immune-related lncRNAs for clinical applications should be determined through functional studies to increase the authenticity of the conclusion. Taken together, the results of our study contribute to the existing understanding of tumor immunity and provide the theoretical groundwork for personalized therapy in clinical TNBC patients.

Conclusions

In summary, we have successfully identified and validated a lncRNA model consisting of eight immune-related lncRNAs. The model holds great promise as a biomarker to assess immune status and predict therapeutic responses in patients with TNBC. Additionally, we demonstrated the novel and crucial role of the LINC01550 molecule in the development of TNBC.

Acknowledgements

This research was funded by the National Natural Science Foundation of China (NSFC) (Grant Nos. 82272049, 82303979).

Disclosure of conflict of interest

None.

Address correspondence to: Drs. Haidong Zhao, Bo Pan and Jun Li, Department of Breast Surgery, The Second Affiliated Hospital of Dalian Medical University, Dalian, Liaoning, China. E-mail: haidong@dmu.edu.cn; z.hddl@hotmail.com (HDZ); bopan@dmu.edu.cn (BP); dyeylj@hotmail.com (JL)

References

[1] Bianchini G, De Angelis C, Licata L and Gianni L. Treatment landscape of triple-negative breast cancer - expanded options, evolving needs. Nat Rev Clin Oncol 2022; 19: 91-113.

[2] Li X, Yang J, Peng L, Sahin AA, Huo L, Ward KC, O'Regan R, Torres MA and Meisel JL. Triple-negative breast cancer has worse overall survival and cause-specific survival than non-triple-negative breast cancer. Breast Cancer Res Treat 2017; 161: 279-287.

[3] Galon J and Bruni D. Approaches to treat immune hot, altered and cold tumours with combination immunotherapies. Nat Rev Drug Discov 2019; 18: 197-218.

[4] Binnewies M, Roberts EW, Kersten K, Chan V, Fearon DF, Merad M, Coussens LM, Gabrilovich DI, Ostrand-Rosenberg S, Hedrick CC, Vonderheide RH, Pittet MJ, Jain RK, Zou W, Howcroft TK, Woodhouse EC, Weinberg RA and Krummel MF. Understanding the tumor immune microenvironment (TIME) for effective therapy. Nat Med 2018; 24: 541-550.

[5] Vonderheide RH. CD40 agonist antibodies in cancer immunotherapy. Annu Rev Med 2020; 71: 47-58.

[6] Yang J, Liu F, Wang Y, Qu L and Lin A. LncRNAs in tumor metabolic reprogramming and immune microenvironment remodeling. Cancer Lett 2022; 543: 215798.

[7] Peltier DC, Roberts A and Reddy P. LNCing RNA to immunity. Trends Immunol 2022; 43: 478-495.

[8] Zhang Y and Cao X. Long noncoding RNAs in innate immunity. Cell Mol Immunol 2016; 13: 138-147.

[9] Zhang H, Zhang N, Wu W, Zhou R, Li S, Wang Z, Dai Z, Zhang L, Liu Z, Zhang J, Luo P, Liu Z and Cheng Q. Machine learning-based tumor-infiltrating immune cell-associated lncRNAs for predicting prognosis and immunotherapy response in patients with glioblastoma. Brief Bioinform 2022; 23: bbac386.

[10] Adewunmi O, Shen Y, Zhang XH and Rosen JM. Targeted inhibition of lncRNA Malat1 alters the tumor immune microenvironment in preclinical syngeneic mouse models of triple-negative breast cancer. Cancer Immunol Res 2023; 11: 1462-1479.

[11] Li G, Kryczek I, Nam J, Li X, Li S, Li J, Wei S, Grove S, Vatan L, Zhou J, Du W, Lin H, Wang T, Subramanian C, Moon JJ, Cieslik M, Cohen M and Zou W. LIMIT is an immunogenic lncRNA in cancer immunity and immunotherapy. Nat Cell Biol 2021; 23: 526-537.

[12] Wang Y, Zhao Y, Guo W, Yadav GS, Bhaskarla C, Wang Z, Wang X, Li S, Wang Y, Chen Y, Pattarayan D, Xie W, Li S, Lu B, Kammula US, Zhang M and Yang D. Genome-wide gain-of-function screening characterized lncRNA regulators for tumor immune response. Sci Adv 2022; 8: eadd0005.

[13] Peng GL, Li L, Guo YW, Yu P, Yin XJ, Wang S and Liu CP. CD8+ cytotoxic and FoxP3+ regulatory T lymphocytes serve as prognostic factors in

breast cancer. Am J Transl Res 2019; 11: 5039-5053.
[14] Fares M, Ayoub NM, Marji R, Al Bashir SM and Al-Shari OM. The impact of tumor-infiltrating lymphocytes on tumor features and pathological characteristics in breast cancer patients: the role of cytotoxic T lymphocytes and regulatory T cells. Eur Rev Med Pharmacol Sci 2022; 26: 4207-4219.
[15] Tang L, Chen Y, Chen H, Jiang P, Yan L, Mo D, Tang X and Yan F. DCST1-AS1 promotes TGF-β-induced epithelial-mesenchymal transition and enhances chemoresistance in triple-negative breast cancer cells via ANXA1. Front Oncol 2020; 10: 280.
[16] Pei X, Wang X and Li H. LncRNA SNHG1 regulates the differentiation of Treg cells and affects the immune escape of breast cancer via regulating miR-448/IDO. Int J Biol Macromol 2018; 118: 24-30.
[17] Durinck S, Spellman PT, Birney E and Huber W. Mapping identifiers for the integration of genomic datasets with the R/Bioconductor package biomaRt. Nat Protoc 2009; 4: 1184-1191.
[18] Li Y, Jiang T, Zhou W, Li J, Li X, Wang Q, Jin X, Yin J, Chen L, Zhang Y, Xu J and Li X. Pan-cancer characterization of immune-related lncRNAs identifies potential oncogenic biomarkers. Nat Commun 2020; 11: 1000.
[19] Wilkerson MD and Hayes DN. ConsensusClusterPlus: a class discovery tool with confidence assessments and item tracking. Bioinformatics 2010; 26: 1572-1573.
[20] Charrad M, Ghazzali N, Boiteau V and Niknafs A. NbClust: an R package for determining the relevant number of clusters in a data set. J Stat Softw 2014; 61: 1-36.
[21] Ru B, Wong CN, Tong Y, Zhong JY, Zhong SSW, Wu WC, Chu KC, Wong CY, Lau CY, Chen I, Chan NW and Zhang J. TISIDB: an integrated repository portal for tumor-immune system interactions. Bioinformatics 2019; 35: 4200-4202.
[22] Hänzelmann S, Castelo R and Guinney J. GSVA: gene set variation analysis for microarray and RNA-seq data. BMC Bioinformatics 2013; 14: 7.
[23] Yoshihara K, Shahmoradgoli M, Martínez E, Vegesna R, Kim H, Torres-Garcia W, Treviño V, Shen H, Laird PW, Levine DA, Carter SL, Getz G, Stemke-Hale K, Mills GB and Verhaak RG. Inferring tumour purity and stromal and immune cell admixture from expression data. Nat Commun 2013; 4: 2612.
[24] Yoshihara K, Kim H and Verhaak RG. Estimate: estimate of stromal and immune cells in malignant tumor tissues from expression data. R package version 1.0.13/r21 2016; <https://R-Forge.R-project.org/projects/estimate/>.
[25] Li T, Fu J, Zeng Z, Cohen D, Li J, Chen Q, Li B and Liu XS. TIMER2.0 for analysis of tumor-infiltrating immune cells. Nucleic Acids Res 2020; 48: W509-W514.
[26] Liu S, Wang Z, Zhu R, Wang F, Cheng Y and Liu Y. Three differential expression analysis methods for RNA sequencing: limma, EdgeR, DESeq2. J Vis Exp 2021.
[27] Wu T, Hu E, Xu S, Chen M, Guo P, Dai Z, Feng T, Zhou L, Tang W, Zhan L, Fu X, Liu S, Bo X and Yu G. clusterProfiler 4.0: a universal enrichment tool for interpreting omics data. Innovation (Camb) 2021; 2: 100141.
[28] Zhang J. GseaVis: implement for 'GSEA' enrichment visualization. R package version 0.0.5 2022; <https://CRAN.R-project.org/package=GseaVis>.
[29] Langfelder P and Horvath S. WGCNA: an R package for weighted correlation network analysis. BMC Bioinformatics 2008; 9: 559.
[30] Langfelder P and Horvath S. Fast R functions for robust correlations and hierarchical clustering. J Stat Softw 2012; 46: i11.
[31] Kassambara A, Kosinski M and Biecek P. Survminer: drawing survival curves using 'ggplot2'. R package version 0.4.9 2021; <https://CRAN.R-project.org/package=survminer>.
[32] Maeser D. OncoPredict: drug and biomarker discovery. R package version 0.2 2021; <https://CRAN.R-project.org/package=oncoPredict>.
[33] Mayakonda A, Lin DC, Assenov Y, Plass C and Koeffler HP. Maftools: efficient and comprehensive analysis of somatic variants in cancer. Genome Res 2018; 28: 1747-1756.
[34] Hao Y, Hao S, Andersen-Nissen E, Mauck WM 3rd, Zheng S, Butler A, Lee MJ, Wilk AJ, Darby C, Zager M, Hoffman P, Stoeckius M, Papalexi E, Mimitou EP, Jain J, Srivastava A, Stuart T, Fleming LM, Yeung B, Rogers AJ, McElrath JM, Blish CA, Gottardo R, Smibert P and Satija R. Integrated analysis of multimodal single-cell data. Cell 2021; 184: 3573-3587, e3529.
[35] McGinnis CS, Murrow LM and Gartner ZJ. DoubletFinder: doublet detection in single-cell RNA sequencing data using artificial nearest neighbors. Cell Syst 2019; 8: 329-337, e324.
[36] Korsunsky I, Millard N, Fan J, Slowikowski K and Raychaudhuri S. Harmony: fast, sensitive, and accurate integration of single cell data. R package version 0.1.1 2022; <https://CRAN.R-project.org/package=harmony>.
[37] Hu C, Li T, Xu Y, Zhang X, Li F, Bai J, Chen J, Jiang W, Yang K, Ou Q, Li X, Wang P and Zhang Y. CellMarker 2.0: an updated database of manually curated cell markers in human/mouse and web tools based on scRNA-seq data. Nucleic Acids Res 2023; 51: D870-D876.

[38] Chu T, Wang Z, Pe'er D and Danko CG. Cell type and gene expression deconvolution with BayesPrism enables Bayesian integrative analysis across bulk and single-cell RNA sequencing in oncology. Nat Cancer 2022; 3: 505-517.
[39] Sun D. Scissor: Single-Cell Identification of Subpopulations with bulk Sample phenOtype coRrelation (SCISSOR). R package version 2.0.0 2022; <https://github.com/sunduanchen/Scissor>.
[40] Liu Y, Pan B, Qu W, Cao Y, Li J and Zhao H. Systematic analysis of the expression and prognosis relevance of FBXO family reveals the significance of FBXO1 in human breast cancer. Cancer Cell Int 2021; 21: 130.
[41] Xiao Y, Ma D, Zhao S, Suo C, Shi J, Xue MZ, Ruan M, Wang H, Zhao J, Li Q, Wang P, Shi L, Yang WT, Huang W, Hu X, Yu KD, Huang S, Bertucci F, Jiang YZ and Shao ZM; AME Breast Cancer Collaborative Group. Multi-omics profiling reveals distinct microenvironment characterization and suggests immune escape mechanisms of triple-negative breast cancer. Clin Cancer Res 2019; 25: 5002-5014.
[42] Lei X, Lei Y, Li JK, Du WX, Li RG, Yang J, Li J, Li F and Tan HB. Immune cells within the tumor microenvironment: biological functions and roles in cancer immunotherapy. Cancer Lett 2020; 470: 126-133.
[43] Piovesan A, Antonaros F, Vitale L, Strippoli P, Pelleri MC and Caracausi M. Human protein-coding genes and gene feature statistics in 2019. BMC Res Notes 2019; 12: 315.
[44] Luo D, Liang Y, Wang Y, Ye F, Jin Y, Li Y, Han D, Wang Z, Chen B, Zhao W, Wang L, Chen X, Jiang L and Yang Q. Long non-coding RNA MIDEAS-AS1 inhibits growth and metastasis of triple-negative breast cancer via transcriptionally activating NCALD. Breast Cancer Res 2023; 25: 109.
[45] Wang Y, Wu S, Zhu X, Zhang L, Deng J, Li F, Guo B, Zhang S, Wu R, Zhang Z, Wang K, Lu J and Zhou Y. LncRNA-encoded polypeptide ASRPS inhibits triple-negative breast cancer angiogenesis. J Exp Med 2020; 217: jem.20190950.
[46] Zhou C, Wang D, Li J, Wang Q, Wo L, Zhang X, Hu Z, Wang Z, Zhan M, He M, Hu G, Chen X, Shen K, Chen GQ and Zhao Q. TGFB2-AS1 inhibits triple-negative breast cancer progression via interaction with SMARCA4 and regulating its targets TGFB2 and SOX2. Proc Natl Acad Sci U S A 2022; 119: e2117988119.
[47] Hu J, Huang H, Xi Z, Ma S, Ming J, Dong F, Guo H, Zhang H, Zhao E, Yao G, Yang L, Zhang F, Zheng W, Chen H, Huang T and Li L. LncRNA SEMA3B-AS1 inhibits breast cancer progression by targeting miR-3940/KLLN axis. Cell Death Dis 2022; 13: 800.
[48] Huang D, Chen J, Yang L, Ouyang Q, Li J, Lao L, Zhao J, Liu J, Lu Y, Xing Y, Chen F, Su F, Yao H, Liu Q, Su S and Song E. NKILA lncRNA promotes tumor immune evasion by sensitizing T cells to activation-induced cell death. Nat Immunol 2018; 19: 1112-1125.
[49] Hong W, Liang L, Gu Y, Qi Z, Qiu H, Yang X, Zeng W, Ma L and Xie J. Immune-related lncRNA to construct novel signature and predict the immune landscape of human hepatocellular carcinoma. Mol Ther Nucleic Acids 2020; 22: 937-947.
[50] Zhao X, Wu P, Liu D, Li C, Xue L, Liu Z, Zhu M, Yang J, Chen Z, Li Y and She Y. An immunity-associated lncRNA signature for predicting prognosis in gastric adenocarcinoma. J Healthc Eng 2022; 2022: 3035073.
[51] Liu CQ, Xia QD, Sun JX, Xu JZ, Lu JL, Liu Z, Hu J and Wang SG. Identification and validation of a twelve immune infiltration-related lncRNA prognostic signature for bladder cancer. Aging (Albany NY) 2022; 14: 1492-1507.
[52] Ramos-Esquivel A, Hernández-Steller H, Savard MF and Landaverde DU. Cyclin-dependent kinase 4/6 inhibitors as first-line treatment for post-menopausal metastatic hormone receptor-positive breast cancer patients: a systematic review and meta-analysis of phase III randomized clinical trials. Breast Cancer 2018; 25: 479-488.
[53] Deng Y, Ma G, Li W, Wang T, Zhao Y and Wu Q. CDK4/6 inhibitors in combination with hormone therapy for HR(+)/HER2(-) advanced breast cancer: a systematic review and meta-analysis of randomized controlled trials. Clin Breast Cancer 2018; 18: e943-e953.
[54] Goel S, DeCristo MJ, Watt AC, BrinJones H, Sceneay J, Li BB, Khan N, Ubellacker JM, Xie S, Metzger-Filho O, Hoog J, Ellis MJ, Ma CX, Ramm S, Krop IE, Winer EP, Roberts TM, Kim HJ, McAllister SS and Zhao JJ. CDK4/6 inhibition triggers anti-tumour immunity. Nature 2017; 548: 471-475.
[55] Teo ZL, Versaci S, Dushyanthen S, Caramia F, Savas P, Mintoff CP, Zethoven M, Virassamy B, Luen SJ, McArthur GA, Phillips WA, Darcy PK and Loi S. Combined CDK4/6 and PI3Kα inhibition is synergistic and immunogenic in triple-negative breast cancer. Cancer Res 2017; 77: 6340-6352.
[56] Evison BJ, Sleebs BE, Watson KG, Phillips DR and Cutts SM. Mitoxantrone, more than just another topoisomerase II poison. Med Res Rev 2016; 36: 248-299.
[57] Li C, Cui J, Wang C, Li Y, Zhang H, Wang J, Li Y, Zhang L, Zhang L, Guo W and Wang Y. Encapsulation of mitoxantrone into pegylated SUVs enhances its antineoplastic efficacy. Eur J Pharm Biopharm 2008; 70: 657-665.

[58] Michaud M, Martins I, Sukkurwala AQ, Adjemian S, Ma Y, Pellegatti P, Shen S, Kepp O, Scoazec M, Mignot G, Rello-Varona S, Tailler M, Menger L, Vacchelli E, Galluzzi L, Ghiringhelli F, di Virgilio F, Zitvogel L and Kroemer G. Autophagy-dependent anticancer immune responses induced by chemotherapeutic agents in mice. Science 2011; 334: 1573-1577.

[59] Tang W, Chen Z, Zhang W, Cheng Y, Zhang B, Wu F, Wang Q, Wang S, Rong D, Reiter FP, De Toni EN and Wang X. The mechanisms of sorafenib resistance in hepatocellular carcinoma: theoretical basis and therapeutic aspects. Signal Transduct Target Ther 2020; 5: 87.

[60] Denkert C, von Minckwitz G, Darb-Esfahani S, Lederer B, Heppner BI, Weber KE, Budczies J, Huober J, Klauschen F, Furlanetto J, Schmitt WD, Blohmer JU, Karn T, Pfitzner BM, Kümmel S, Engels K, Schneeweiss A, Hartmann A, Noske A, Fasching PA, Jackisch C, van Mackelenbergh M, Sinn P, Schem C, Hanusch C, Untch M and Loibl S. Tumour-infiltrating lymphocytes and prognosis in different subtypes of breast cancer: a pooled analysis of 3771 patients treated with neoadjuvant therapy. Lancet Oncol 2018; 19: 40-50.

[61] Stanton SE and Disis ML. Clinical significance of tumor-infiltrating lymphocytes in breast cancer. J Immunother Cancer 2016; 4: 59.

[62] Lu Y, Zhao Q, Liao JY, Song E, Xia Q, Pan J, Li Y, Li J, Zhou B, Ye Y, Di C, Yu S, Zeng Y and Su S. Complement signals determine opposite effects of B cells in chemotherapy-induced immunity. Cell 2020; 180: 1081-1097, e1024.

[63] Montfort A, Pearce O, Maniati E, Vincent BG, Bixby L, Böhm S, Dowe T, Wilkes EH, Chakravarty P, Thompson R, Topping J, Cutillas PR, Lockley M, Serody JS, Capasso M and Balkwill FR. A strong B-cell response is part of the immune landscape in human high-grade serous ovarian metastases. Clin Cancer Res 2017; 23: 250-262.

[64] Vito A, Salem O, El-Sayes N, MacFawn IP, Portillo AL, Milne K, Harrington D, Ashkar AA, Wan Y, Workenhe ST, Nelson BH, Bruno TC and Mossman KL. Immune checkpoint blockade in triple negative breast cancer influenced by B cells through myeloid-derived suppressor cells. Commun Biol 2021; 4: 859.

[65] Drobits B, Holcmann M, Amberg N, Swiecki M, Grundtner R, Hammer M, Colonna M and Sibilia M. Imiquimod clears tumors in mice independent of adaptive immunity by converting pDCs into tumor-killing effector cells. J Clin Invest 2012; 122: 575-585.

[66] Kalb ML, Glaser A, Stary G, Koszik F and Stingl G. TRAIL(+) human plasmacytoid dendritic cells kill tumor cells in vitro: mechanisms of imiquimod- and IFN-α-mediated antitumor reactivity. J Immunol 2012; 188: 1583-1591.

[67] Yoneyama H, Matsuno K, Toda E, Nishiwaki T, Matsuo N, Nakano A, Narumi S, Lu B, Gerard C, Ishikawa S and Matsushima K. Plasmacytoid DCs help lymph node DCs to induce anti-HSV CTLs. J Exp Med 2005; 202: 425-435.

Figure S1. Immune infiltration analysis from TIMER2.0 database.

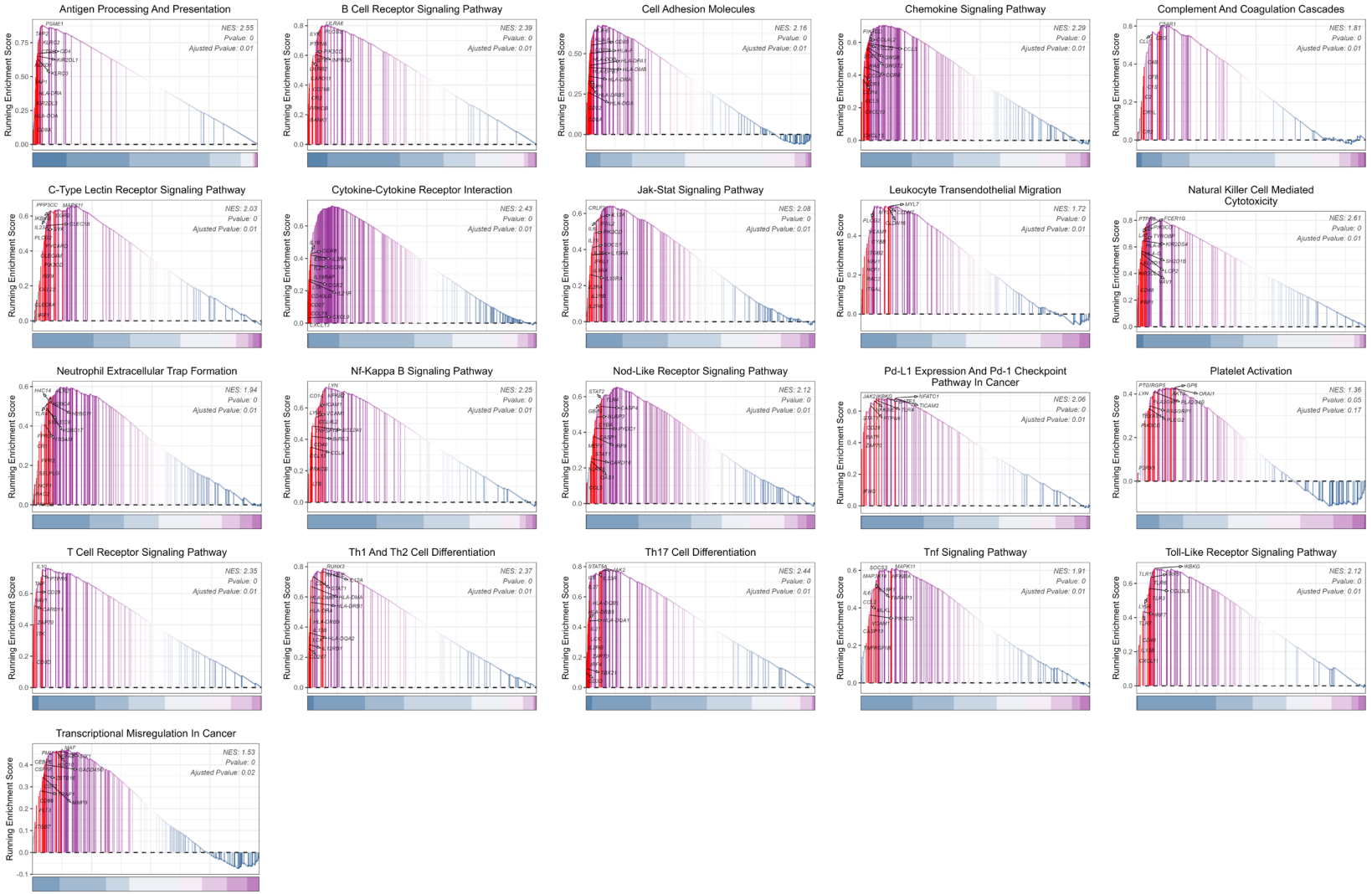

Figure S2. GSEA analysis of immune and inflammatory related pathways in “cold” and “hot” clusters of TNBC.

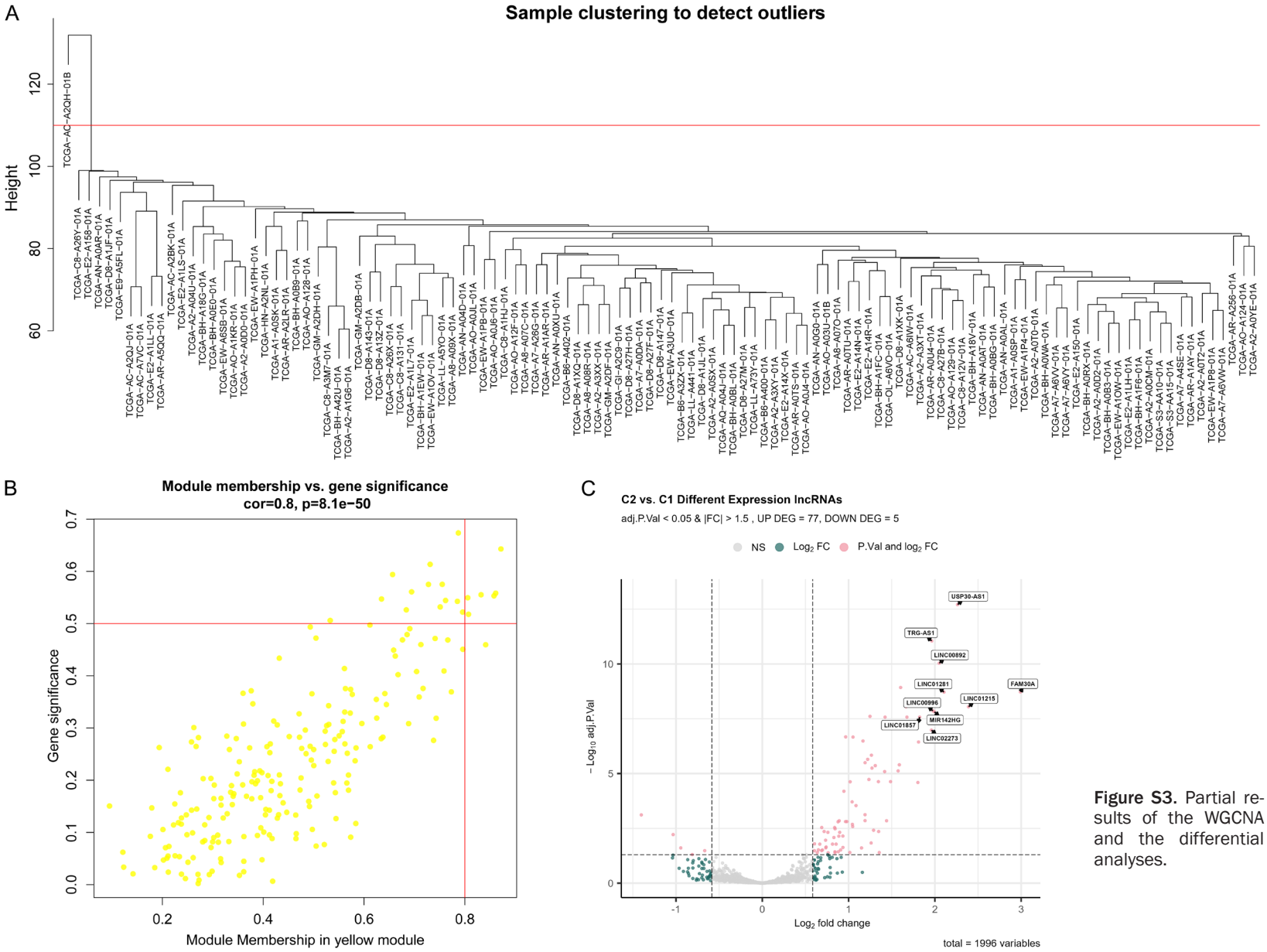

Figure S3. Partial results of the WGCNA and the differential analyses.

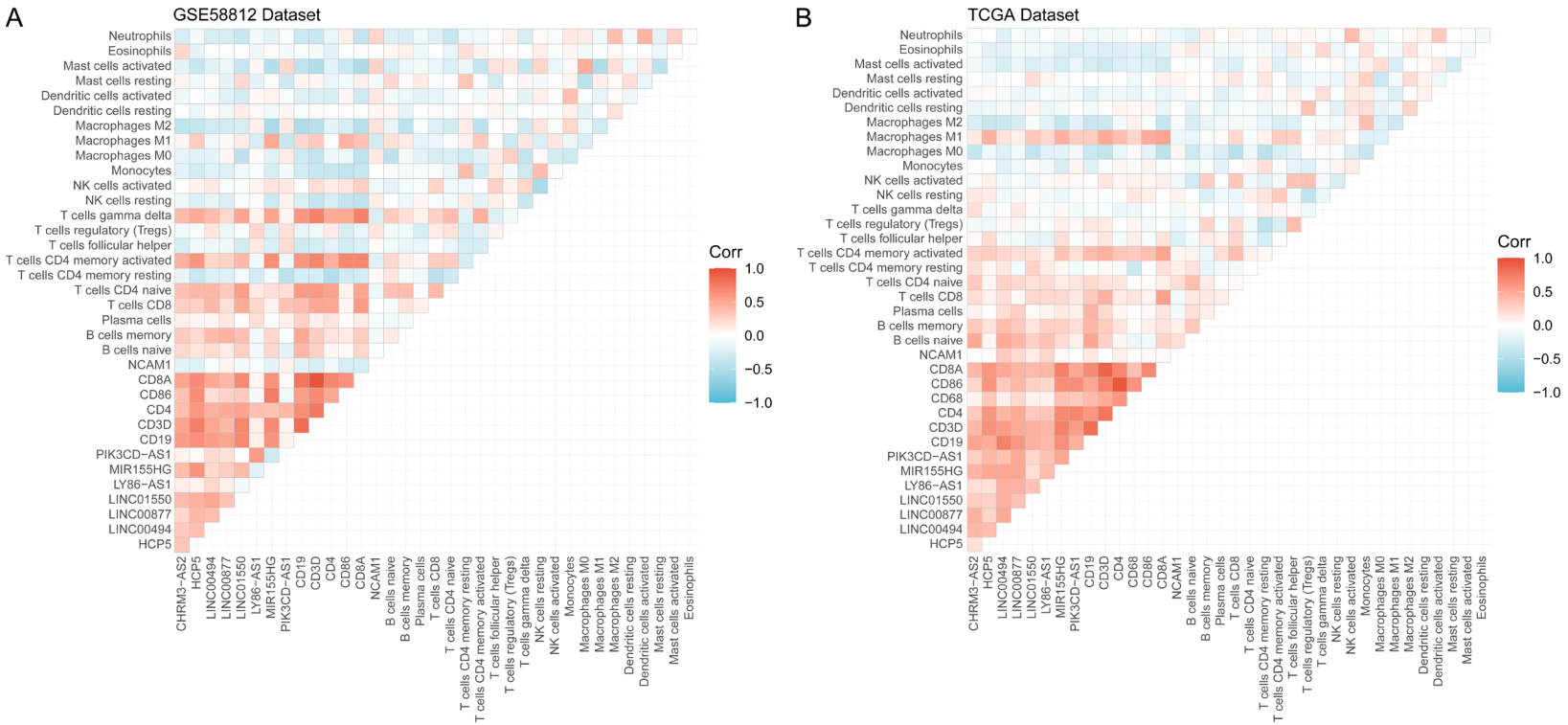

Figure S4. Correlation heatmaps of immune-related lncRNAs and infiltrating immune cells.

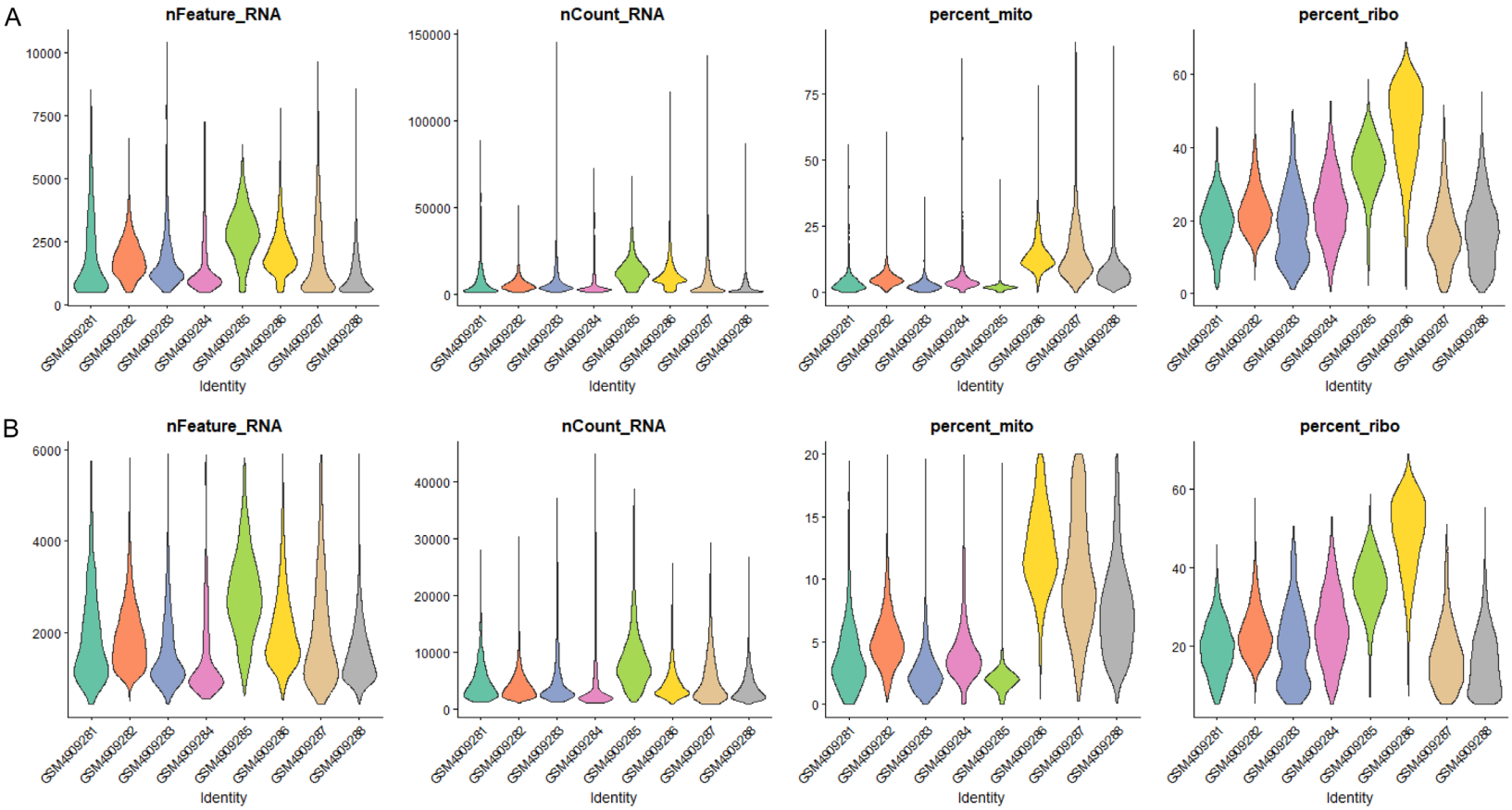
A
nFeature_RNA
nCount_RNA
percent_mito
percent_ribo
B
nFeature_RNA
nCount_RNA
percent_mito
percent_ribo
Identity
GSM4909281
GSM4909282
GSM4909283
GSM4909284
GSM4909285
GSM4909286
GSM4909287
GSM4909288

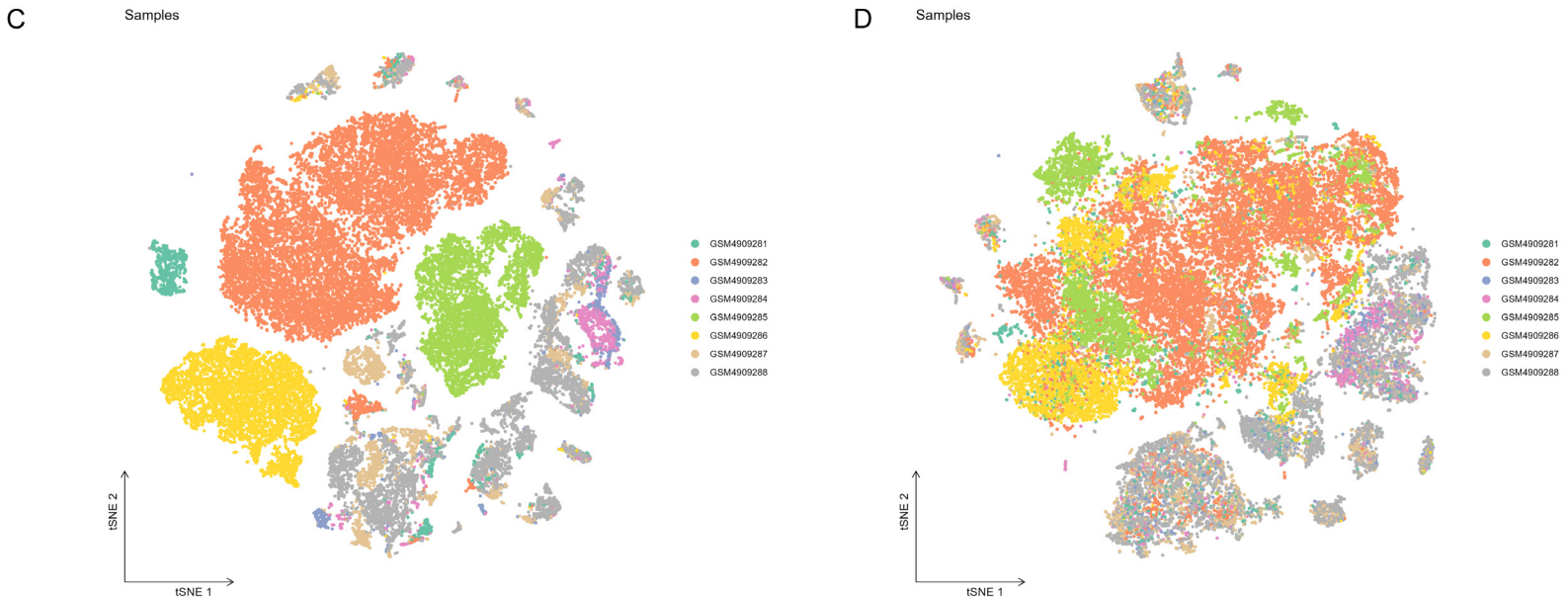

Figure S5. The preprocessing results of single-cell RNA sequencing data in GSE161529 dataset.